Regulation of transcriptional bursting by core promoter elements in the *Drosophila* embryo

Moe Yokoshi[1], Manuel Cambón[2], Takashi Fukaya[1,3*]

[1] Laboratory of Transcription Dynamics, Research Center for Biological Visualization, Institute for Quantitative Biosciences, The University of Tokyo, Bunkyo-ku, Tokyo, Japan

[2]Applied Mathematics Department, University of Granada, Granada, Spain

[3]Department of Life Sciences, Graduate School of Arts and Sciences, The University of Tokyo, Bunkyo-ku, Tokyo, Japan

*Correspondence should be addressed to T.F

Tel: +81 3 5841 1453

E-mail: tfukaya@iqb.u-tokyo.ac.jp

Abstract

Transcriptional bursting is a pervasive feature of gene expression conserved across species, but its mechanism is poorly understood. Here, we provide evidence that core promoter elements regulate transcriptional bursting at multiple levels in early *Drosophila* embryos. Quantitative live imaging analysis revealed that downstream core promoter elements contribute to regulation of bursting frequency. In contrast, the upstream TATA box mainly impacts amplitude of transcriptional bursting. Genome editing analysis further revealed that burst regulation by endogenous TATA box and downstream core promoter elements is essential for the spatial patterning of key developmental genes. We suggest that core promoter elements serve as a key regulatory module in converting enhancer activity into transcriptional bursting during animal development.

Introduction

Transcriptional bursting is emerging as a pervasive feature of gene expression conserved across species (*e.g.*, Bothma *et al*, 2014; Chong *et al*, 2014; Chubb *et al*, 2006; Larson *et al*, 2011; Lee *et al*, 2019; Little *et al*, 2013; Pare *et al*, 2009; Raj *et al*, 2006; Suter *et al*, 2011; Zenklusen *et al*, 2008). It is thought to arise from consecutive recruitment and release of multiple RNA polymerase II (Pol II) complexes followed by a refractory period, resulting in successive bursts of *de novo* transcription. This phenomenon was directly visualized more than 40 years ago in electron micrographs of chromatin spreads in early *Drosophila* embryos, in which active transcription units are separated by internal fiber-free gaps (McKnight & Miller, 1979). Recent quantitative imaging studies suggested that enhancers regulate the frequency of transcriptional bursting (Bartman *et al*, 2016; Fukaya *et al*, 2016; Larsson *et al*, 2019). However, considerably less is known about the role of core promoters in the process.

Core promoters are short segments of DNA, which typically range -40 to +40 relative to the +1 transcription start site (TSS). They serve as a docking site for general transcription factors and Pol II for assembly of the pre-initiation complex (PIC). Initiation of transcription also requires sequence-specific transcription factors and coactivators bound to enhancers. Thus, core promoters act as a "gateway to transcription", converting enhancer activity into gene expression (reviewed in Vo Ngoc *et al*, 2019).

Core promoters consist of several sequence motifs located at fixed positions relative to the TSS. The TATA box (TATA) (Goldberg, 1979) is typically located 25 to 30 bp upstream of the TSS and directly interacts with TATA-binding protein (TBP), a subunit of the transcription factor IID (TFIID) complex. Initiator (Inr), motif 10 element (MTE), and downstream core promoter element (DPE) are sequence motifs downstream of TATA (Burke & Kadonaga, 1996; Lim *et al*, 2004; Smale & Baltimore, 1989) and serve as an additional docking site for TFIID via direct interaction with TBP-associating factors (TAFs) (Burke & Kadonaga, 1997; Chalkley & Verrijzer, 1999; Louder *et al*, 2016; Patel *et al*, 2018; Theisen *et al*, 2010). The precise composition of core promoter elements varies substantially among Pol II-transcribed genes (Chen *et al*, 2014; FitzGerald *et al*, 2006; Ohler *et al*, 2002), which is thought to play a key role in the regulation of enhancer-promoter interaction and gene expression (Butler & Kadonaga, 2001; Ohtsuki *et al*, 1998; Zabidi *et al*, 2015).

In this study, we systematically visualized the role of individual core promoter elements using MS2/MCP live imaging method in developing *Drosophila* embryos (Garcia *et al*, 2013; Lucas *et al*, 2013). Quantitative image analysis suggests that downstream elements alter the frequency of transcriptional bursting even under the control of a fixed enhancer. In contrast, the upstream TATA was found to largely affect bursting amplitude. To dissect the function of core promoter elements in the context of the endogenous genome, we developed a gene complementation approach by combining genome editing and site-directed transgenesis. Using the key developmental patterning gene *fushi tarazu* (*ftz*), we show that both TATA and DPE mutations lead to misregulation of bursting activities, resulting in disrupted spatial patterning of gene expression and severe defects including expression of the downstream segment polarity gene *engrailed* (*en*). Our data suggest that core promoter elements serve as a key regulatory module in the control of transcriptional bursting during animal development.

Result and discussion

To examine how core promoter elements regulate transcriptional bursting, we used the MS2/MCP live-imaging method in early *Drosophila* embryos (Garcia *et al.*, 2013; Lucas *et al.*, 2013). We constructed a reporter system in which the *yellow* gene was placed under the control of the well-characterized *Drosophila* synthetic core promoter (DSCP), a modified *even-skipped* (*eve*) core promoter containing TATA, Inr, MTE, and DPE at optimal positions relative to the TSS (Fig 1A and Fig EV1A) (Pfeiffer *et al*, 2008). A 24x MS2 RNA stem-loop sequence was engineered into the 5′ untranslated region (UTR) to enable visualization of nascent RNA production with a maternally provided MCP-GFP fusion protein. *DSCP-MS2-yellow* reporter gene was placed under the control of a full-length 1.5-kb *snail* (*sna*) shadow enhancer (Fig 1B), which drives expression in the ventral region of early embryos (Dunipace *et al*, 2011; Perry *et al*, 2010). In this synthetic locus, *sna* shadow enhancer is located ~6.5 kb away from the TSS, which is similar to the enhancer-promoter distance found at the endogenous *sna* locus (~7 kb). Transgenes were integrated into a specific genomic landing site via phiC31-mediated transgenesis (Groth *et al*, 2004; Venken *et al*, 2006).

First, we examined the downstream core promoter elements Inr, MTE and DPE by introducing mutations that compromise their direct interaction with TFIID (Fig 1C) (Burke & Kadonaga, 1996, 1997; Kutach & Kadonaga, 2000; Lim *et al.*, 2004; Theisen *et al.*, 2010). Notably, the mutation at the +18 to +22 positions eliminates MTE-dependent transcription without affecting DPE function (Lim *et al.*, 2004; Theisen *et al.*, 2010), allowing us to examine the individual contributions of MTE and DPE in the same core promoter context. Transcriptional activity was monitored from the entry into nuclear cycle (nc) 14 to the onset of gastrulation. To unambiguously compare the activities of different reporter genes at the same Dorsal-Ventral (DV) position, we focused on the ventral most nuclei, as defined by the location of ventral furrow formation at the onset of gastrulation (Fig 1D). Quantitative image analysis revealed that the MTE mutant (mMTE) produces fewer number of bursts than WT (Fig 1E, Movie EV1). In comparison, the Inr mutant (mInr) and the DPE mutant (mDPE) produced even less frequent bursts than mMTE (Fig 1E, Movie EV1), suggesting that downstream elements can individually contribute to the regulation of bursting frequency, with Inr/DPE playing a major role and MTE playing a more supplemental role. This trend was clearly seen when MS2 trajectories in all analyzed nuclei were visualized as a heat map (Fig 1F). Next, we analyzed individual bursting events and quantified their functional parameters, including

amplitude, duration, and frequency (Fig EV1B). As seen in individual MS2 trajectories (Fig 1E), the frequency of transcriptional bursting and total output were largely diminished upon mutation into downstream elements (Fig 1G). However, when bursts were produced, their duration and amplitude were comparable with those produced from WT (Fig 1G). These data suggest that Inr, MTE and DPE control gene activity mainly by modulating the frequency of transcriptional bursting in early embryos. Essentially same results were observed when *sna* shadow enhancer was replaced with another key developmental enhancer, *rhomboid* neuroectoderm element (*rho*NEE) (Ip *et al*, 1992) (Fig EV2).

We next examined the role of the upstream TATA, which we mutated according to previous characterization in order to abrogate its function (Fig 2A) (Butler & Kadonaga, 2001; Lim *et al.*, 2004). Contrary to downstream elements, live imaging analysis revealed that TATA mutation dramatically diminishes overall transcription activity (Fig 2B, Movie EV2). This trend can be clearly seen in the heat map analysis (Fig 2C). Importantly, bursts produced from the TATA mutant (mTATA) exhibited significantly lower amplitude than WT (Fig 2D), suggesting that TATA mutation largely diminishes the number of Pol II released per burst. The frequency of transcriptional bursting was also reduced by the TATA mutation (Fig 2D). It is conceivable that relatively weak bursts seen in the WT DSCP became undetectable as a consequence of diminished amplitude. Strong TATA-dependency was also observed when *rho*NEE was used for the analysis (Fig EV2). Overall, our data is consistent with the idea that downstream elements and the upstream TATA differentially regulate bursting profiles in *Drosophila* embryos.

In *Drosophila*, core promoters often contain binding sites for sequence-specific DNA binding proteins, Zelda and GAGA factor (GAF) (Harrison *et al*, 2011; Lee *et al*, 2008), that are thought to recruit chromatin remodeling complexes such as NURF to increase chromatin accessibility of regulatory regions (Fuda *et al*, 2015; Sun *et al*, 2015; Tsukiyama & Wu, 1995). DSCP contains a GAF-binding site (GAGA) from the *eve* core promoter (Fig EV1A) (Ohtsuki & Levine, 1998), but lacks any known Zelda binding motifs. To examine how promoter-proximal GAGA and Zelda sites influence transcription dynamics, we either mutagenized GAGA site or added Zelda sites (Fig EV3A). Bursting activities were moderately diminished upon GAGA mutation (Fig EV3B-D). On the other hand, addition of Zelda sites led to rapid induction of transcriptional bursting in a highly synchronous manner (Fig EV3B and C) and an overall increase in the transcriptional output (Fig EV3D). These data suggest that promoter

opening by GAF and Zelda facilitates induction of transcriptional bursting, especially at the onset of nc14.

Previous computational analysis identified Pause button (PB; KCGRWCG) as a core promoter element enriched in genes associated with paused Pol II in early embryos (Hendrix *et al*, 2008). To examine how PB impacts gene activities, we converted the sequence at +26 to +32 positions into an optimal PB motif via A-to-G single nucleotide substitution at +28 position that does not compromise the DPE consensus (Fig EV4A) (Kutach & Kadonaga, 2000). This resulted in only subtle changes in bursting activities (Fig EV4B-D), suggesting that PB has a limited impact in this core promoter context. It has been reported that TATA is typically depleted from paused promoters in *Drosophila* (Chen *et al*, 2013; Gaertner *et al*, 2012; Shao *et al*, 2019). When TATA was mutated in a PB-containing promoter (Fig EV4A), there was a significant reduction in overall transcription activities as in the case of single TATA mutation (Fig EV4B-D). Importantly, we did not see clear accumulation of Pol II at the promoter region of this reporter gene (Fig EV4E). These results implicate that TATA mutation can negatively regulate gene activities independently of Pol II pausing.

To determine how core promoter elements impact enhancer-promoter interactions at the endogenous locus, we next focused on one of the best studied developmental patterning genes, *ftz* (Hafen *et al*, 1984; Kuroiwa *et al*, 1984; Nüsslein-Volhard, 1982; Wakimoto & Kaufman, 1981; Wakimoto *et al*, 1984). *ftz* is expressed in seven transverse stripes spanning across the anterior-posterior (AP) axis and is regulated by multiple enhancers located 5′ and 3′ of the transcription unit (Calhoun & Levine, 2003; Hiromi & Gehring, 1987; Hiromi *et al*, 1985; Pick *et al*, 1990; Schroeder *et al*, 2011). The *ftz* core promoter contains TATA, Inr and DPE elements (Fig 3A) (Juven-Gershon *et al*, 2008). Reporter assays in *Drosophila* S2 cultured cells have suggested that DPE, but not TATA, is specifically required for the activation of the *ftz* core promoter by the homeodomain-containing transcription factor Caudal (Juven-Gershon *et al.*, 2008). In this model, mutation of DPE is expected to most severely affect *ftz* expression in stripe 5 and 6, which are activated by Caudal (Macdonald & Struhl, 1986). To test this idea, we developed a gene complementation approach for visualizing impacts of core promoter modification at the endogenous locus. First, the entire *ftz* transcription unit was replaced with attP site via CRISPR/Cas9-mediated genome editing. Subsequently, a full-length *ftz* transcription unit containing the modified core promoter and 24x MS2 sequence was integrated into the attP site via phiC31-mediated transgenesis (Fig 3B and C).

Fluorescent *in situ* hybridization assay revealed that *ftz* expression is diminished equally across all seven stripes upon DPE mutation (Fig 3D), indicating that the function of DPE is not restricted to Caudal-dependent stripes. Moreover, *ftz* expression was almost completely lost upon TATA mutation (Fig 3D). These data suggest that the correct expression of *ftz* requires both TATA and DPE. To determine functional consequences of irregular *ftz* expression in our mutant embryos, we examined the expression pattern of the segment polarity gene *engrailed* (*en*), which is activated by the Ftz protein in even-numbered stripes (DiNardo & O'Farrell, 1987; Howard & Ingham, 1986). As expected, the WT core promoter *ftz* construct restored *en* expression by producing a full-length Ftz protein (Fig 3E and Fig EV5A). Quantification of hatching rate showed that homozygous lethality of deletion allele was rescued more than 70% of embryos (Fig 3F). Hatching rate was slightly lower than the control (Fig 3F), implicating that extra sequences derived from the plasmid backbone partially affect *ftz* expression (Fig 3C). Importantly, neither the mTATA nor mDPE constructs were able to rescue *en* expression and embryonic lethality (Fig 3E and Fig EV5B). These data indicate that both TATA and DPE are required for *in vivo* functions of *ftz* during embryo segmentation.

To elucidate the molecular basis underlying these phenotypes, we carried out live imaging analysis of individual *ftz-MS2* complementation alleles. We focused on anterior stripe 1/2 and posterior stripe 5/6 (Fig 4A and Movie EV3) because regulatory mechanisms in these regions are well characterized (Carroll & Scott, 1986; Frasch & Levine, 1987; Macdonald & Struhl, 1986; Nüsslein-Volhard *et al*, 1987). While both the mTATA and mDPE *ftz* alleles failed to complement the *ftz* null mutation (Fig 3D and E), their MS2 profiles differ dramatically. The mDPE allele produced discontinuous but strong bursting activity (Fig 4B), whereas the mTATA allele further led to the overall diminishment of MS2 intensity in all analyzed stripes (Fig 4B and 4C). Importantly, these profile changes are similar to our preceding observations at the synthetic locus (Fig 1 and 2, Fig EV2). As a consequence, the mTATA allele exhibited a ~82-89% reduction in the total RNA production, while the mDPE allele showed a more modest reduction (Fig 4D). We then characterized the functional parameters of MS2 trajectories. As we previously reported (Yokoshi *et al*, 2020), individual bursting events were hard to be discerned due to the continuity of bursting activities at the WT *ftz* allele (Fig 4B), suggesting that the endogenous genomic configurations are highly optimized for efficient production of transcriptional bursting within a short period of time. To minimize ambiguity in defining individual bursting events, we quantified the fraction of active nuclei (Fig 4E) and the

mean MS2 intensity in actively transcribing nuclei (Fig 4F). In this analysis, frequent bursts will result in an increased fraction of active nuclei, and high amplitude will result in a high mean intensity. We found that mutation of TATA and DPE equally diminish the fraction of active nuclei in all stripe regions (Fig 4E). On the other hand, the level of MS2 intensity was more severely reduced in the mTATA allele (Fig 4F), suggesting that the TATA mutation reduces the number of Pol II entering into productive elongation even when core promoter is in an active state. Overall, our results are consistent with the idea the TATA and DPE differentially regulate the amplitude and the frequency of transcriptional bursting in early embryos.

Lastly, to determine how misregulation of bursting activities affects the stripe formation, we computationally reconstituted the spatial patterning of *ftz* expression by calculating the total RNA production at each nucleus and the *ftz* mRNA turnover rate in early embryos (half-life: 7 min) (Edgar *et al*, 1986). Although the mDPE allele showed somewhat stronger MS2 activities than the mTATA (Fig 4), both resulted in highly sporadic stripe patterns (Fig EV5C and D). Thus, we concluded that the endogenous configuration of *ftz* core promoter is essential for the uniform expression at the stripe regions, and for proper regulation of downstream genes such as *en* (Fig 3E)

In this study, we provided evidence that each core promoter element can differentially regulate transcriptional bursting in early *Drosophila* embryos. Our data suggests that the downstream elements, Inr, MTE and DPE individually modulate the frequency of transcriptional bursting without largely affecting the amplitude or duration (Fig 1). On the other hand, TATA mutation dramatically diminished overall transcription activity including the bursting amplitude (Fig 2). Importantly, recent cryo-EM analysis has revealed that TFIID recognizes the core promoter in a stepwise fashion (Cianfrocco *et al*, 2013; Louder *et al.*, 2016; Patel *et al.*, 2018), with initial contact with Inr, MTE and DPE through TAF1/2 subunits, followed by dynamic structural rearrangement that facilitates recognition of the upstream TATA by TBP. We speculate that the rate of initial TFIID loading onto the downstream core promoter region mainly affects the bursting frequency, and the subsequent TBP loading onto the upstream TATA regulates the bursting amplitude and the frequency (Fig 5). This step-wise mechanism may help to diversify core promoter activities across the genome because there are substantial variations in composition of core promoter elements among Pol II-transcribed genes. For example, it is estimated that only a small fraction of protein coding genes contain TATA, both in human and *Drosophila* (Chen *et al.*, 2014; FitzGerald *et al.*, 2006; Ohler *et al.*, 2002). As

suboptimal transcription factor binding sites are important for tissue-specific gene activation by enhancers (Crocker *et al*, 2015; Farley *et al*, 2015), suboptimal core promoters might play a key role for ensuring the spatial and temporal specificity of gene expression during animal development. In this study, we engineered core promoter elements by introducing mutations that alternate entire sequences within individual motifs. Future functional studies are needed to fully elucidate the roles of core promoters by analyzing intermediates between the most optimized and dysregulated motifs in the context of various core promoter sequences.

Regulation of transcriptional bursting by core promoter elements seems to be a common mechanism conserved across species. Analysis of actin genes in *Dictyostelium* showed that swapping of entire promoter regions can alter activity of transcriptional bursting (Tunnacliffe *et al*, 2018), although it remains to be determined which core promoter elements are specifically responsible for the burst regulation in this system. Intriguingly, recent live imaging studies showed that transcriptional bursts are often separated by refractory period of several hours in mammalian systems (*e.g.,* Molina *et al*, 2013; Nicolas *et al*, 2018; Rodriguez *et al*, 2019; Suter *et al.*, 2011). Recent single-cell RNA-seq and reporter gene studies suggested that TATA and Inr affect hour-scale bursting activities in mouse and human cultured cells (Larsson *et al.*, 2019; Tantale *et al*, 2016). Our data suggest that *Drosophila* embryos use core promoter elements to regulate bursting activities at finer time-scale, which may help to establish dynamic ON/OFF patterns of gene expression during rapid processes of embryogenesis.

Figure Legends

Figure 1. Downstream elements regulate frequency of transcriptional bursting.
(A) Schematic representation of the *Drosophila* synthetic core promoter (DSCP).
(B) Schematic representation of the *yellow* reporter gene containing the 155-bp DSCP, the 1.5-kb *sna* shadow enhancer, and 24x MS2 RNA stem loops (Bertrand *et al*, 1998) within the 5′ UTR.
(C) Inr, MTE and DPE were mutated as indicated.
(D) Snapshot of a gastrulating embryo (left) and false-coloring of ventral most nuclei at mid nc14 (right). The maximum projected image of His2Av-mRFP is shown in gray. Images are oriented with ventral view facing up. Scale bar indicates 20 μm.
(E) A representative trajectory of transcription activity of the MS2 reporter genes with WT DSCP (left), mInr DSCP (middle left), mMTE DSCP (middle right) and mDPE DSCP (right) in individual nuclei.
(F) MS2 trajectories for all analyzed nuclei. Each row represents the MS2 trajectory for a single nucleus. A total of 403, 435, 509 and 444 ventral most nuclei, respectively, were analyzed from three independent embryos for the reporter genes with WT DSCP (left), mInr DSCP (middle left), mMTE DSCP (middle right) and mDPE DSCP (right). All analyzed nuclei for each experiment were ordered by their onset of transcription in nc14.
(G) Boxplots showing the distribution of total output (left), burst amplitude (middle left), burst duration (middle right) and burst frequency (right). The box indicates the lower (25%) and upper (75%) quantile and the solid line indicates the median. Whiskers extend to the most extreme, non-outlier data points. A total of 403, 435, 509 and 444 ventral most nuclei, respectively, were analyzed from three independent embryos for the reporter genes with WT DSCP, mInr DSCP, mMTE DSCP and mDPE DSCP. Relative median values normalized to the WT DSCP reporter are shown in bottom.

Data information: See also Figure EV1, EV2 and Movie EV1.

Figure 2. TATA controls amplitude of transcriptional bursting.
(A) TATA was mutated as indicated.
(B) A representative trajectory of transcription activity of the MS2 reporter genes with WT DSCP (left) and mTATA DSCP (right) in individual nuclei.
(C) MS2 trajectories for all analyzed nuclei. Each row represents the MS2 trajectory for a single nucleus. A total of 401 and 406 ventral most nuclei, respectively, were analyzed from three independent embryos for the reporter genes with WT DSCP (left) and mTATA

DSCP (right). All analyzed nuclei for each experiment were ordered by their onset of transcription in nc14.
(D) Boxplots showing the distribution of total output (left), burst amplitude (middle left), burst duration (middle right) and burst frequency (right). The box indicates the lower (25%) and upper (75%) quantile and the solid line indicates the median. Whiskers extend to the most extreme, non-outlier data points. A total of 401 and 406 ventral most nuclei, respectively, were analyzed from three independent embryos for the reporter genes with WT DSCP (left) and mTATA DSCP (right). Relative median values normalized to the WT DSCP reporter are shown in bottom.

Data information: See also Figure EV2 and Movie EV2.

Figure 3. Both TATA and DPE are required for proper *ftz* expression and function.
(A) *ftz* core promoter contains TATA, Inr and DPE.
(B) TATA and DPE were mutated as indicated.
(C) Schematic representation of the core promoter modification approach. Approximate locations of enhancers regulating *ftz* expression in early embryos are indicated as "E". Note that extra sequences derived from plasmid backbone, ampicillin resistant gene (*ampR*) and mini-white marker gene (*miniW*) were incorporated into the *ftz* locus after phiC31-mediated integration.
(D) Fluorescent *in situ* hybridization of *ftz*. Embryos at late nc14 were shown. *yw* embryo is shown as a control. Images are cropped and rotated to align embryos (anterior to the left and posterior to the right). Scale bar indicates 50 μm.
(E) Fluorescent *in situ* hybridization of *en*. Embryos after germband extension were shown. *yw* embryo is shown as a control. Images are cropped and rotated to align embryos (anterior to the left and posterior to the right). Brightness of each embryo was differentially adjusted for visualization of *en* expression pattern. Scale bar indicates 50 μm.
(F) Hatching rates of eggs laid by *yw* and homozygote WT *ftz-MS2* complementation lines. Each dot represents measurement from a single experiment. For each trial, 500 embryos were analyzed.

Data information: See also Figure EV5.

Figure 4. TATA and DPE differentially regulate *ftz* transcription.
(A, left) False-coloring of nuclei at stripe 1 (cyan) and stripe 2 (blue). (A, right) False-

coloring of nuclei at stripe 5 (cyan) and stripe 6 (blue). The maximum projected image of His2Av-mRFP is shown in gray. Images are oriented with anterior to the left. Scale bar indicates 20 µm.
(B) A representative trajectory of transcription activity of *ftz-MS2* in individual nuclei.
(C) MS2 trajectories for all analyzed nuclei. Each row represents the MS2 trajectory for a single nucleus. A total of 234, 236 and 228 nuclei at stripe 1, 248, 241 and 242 nuclei at stripe 2, 243,238 and 240 nuclei at stripe 5, and 232, 243 and 240 nuclei at stripe 6 were analyzed from three individual embryos for the *ftz-MS2* with WT, mTATA and mDPE core promoter, respectively. All analyzed nuclei for each experiment were ordered by their onset of transcription in nc14.
(D) Boxplot showing the distribution of total output. The box indicates the lower (25%) and upper (75%) quantile and the solid line indicates the median. Whiskers extend to the most extreme, non-outlier data points. A total of 234, 236 and 228 nuclei at stripe 1, 248, 241 and 242 nuclei at stripe 2, 243,238 and 240 nuclei at stripe 5, and 232, 243 and 240 nuclei at stripe 6 were analyzed from three individual embryos for the *ftz-MS2* with WT, mTATA and mDPE core promoter, respectively. Relative median values normalized to the *ftz-MS2* with WT core promoter are shown in bottom.
(E) Fraction of actively transcribing nuclei at each expression domain. A total of 234, 236 and 228 nuclei at stripe 1, 248, 241 and 242 nuclei at stripe 2, 243,238 and 240 nuclei at stripe 5, and 232, 243 and 240 nuclei at stripe 6 were analyzed from three individual embryos for the *ftz-MS2* with WT, mTATA and mDPE core promoter, respectively.
(F) Mean MS2 intensity per actively transcribing nucleus at each expression domain. A total of 234, 236 and 228 nuclei at stripe 1, 248, 241 and 242 nuclei at stripe 2, 243,238 and 240 nuclei at stripe 5, and 232, 243 and 240 nuclei at stripe 6 were analyzed from three individual embryos for the *ftz-MS2* with WT, mTATA and mDPE core promoter, respectively. Error bars represent the standard deviation of the mean across active nuclei at given time.

Data information: See also Figure EV5 and Movie EV3.

Figure 5. Model for burst regulation by core promoter elements.
Individual core promoter elements directly contact with subunits of the TFIID complex. TAF1 and TAF2 subunits interact with Inr, MTE and DPE. This initial interaction induces structural rearrangement of the complex to facilitate subsequent loading of TBP onto TATA (Patel *et al.*, 2018). Inr, MTE and DPE mainly affect the bursting frequency, and TATA affects the bursting amplitude and the frequency.

Acknowledgment

We thank Bomyi Lim and Tyler Heist for sharing nuclei segmentation and tracking code, Hitomi Takishita and Misako Sato for fly husbandry, Tetsuya Tabata for advice on hatching rate analysis, Kota Hamamoto for advice on ChIP-qPCR analysis and the Bloomington *Drosophila* Stock Center for fly strains. We are also grateful to Michael Levine, Tyler Heist, Yuko Hasegawa, Life Science Editors and members of the Fukaya laboratory for critical comments on the manuscript. M.Y is supported by the Grant-in-Aid for Early-Career Scientists (20K15710) from the Japan Society for the Promotion of Science, and the Employment Stability Support for Young Researchers from the University of Tokyo. M.C is supported by the FPI research grant (FPI2015/074837) from the MINECO-Feder, and the FisyMat PhD Student Research program from University of Granada. This study was funded by the Grant-in-Aid for Scientific Research on Innovative Areas (Research in a Proposed Research Area) (20H05357), the Grants-in-Aid for Scientific Research (B) (19H03154), the Grants-in-Aid for Challenging Research (Exploratory) (19K22378), the Grants-in-Aid for Research Activity Start-up (18H06040) from the Japan Society for the Promotion of Science, the Grants-in-Aid for Leading Initiative for Excellent Young Researchers from the Ministry of Education, Culture, Sports, Science and Technology in Japan, Tomizawa Jun-ichi & Keiko Fund of Molecular Biology Society of Japan for Young Scientist, research grants from the Mochida Memorial Foundation for Medical and Pharmaceutical Research, the Nakajima Foundation, the Inamori Foundation, the Takeda Science Foundation, the Sumitomo Foundation and the Senri Life Science Foundation.

Author Contributions

M.Y performed the experiments. M.Y and T.F analyzed the data. M.C developed image analysis code. T.F wrote the manuscript. All the authors discussed the results and approved the manuscript.

Conflict of interest

The authors declare no competing interests

Materials and Methods

Experimental model

In all imaging experiments, we studied *Drosophila melanogaster* embryos at nuclear cycle 14 unless otherwise noted. The following fly lines were used in this study: *nanos>MCP-GFP, His2Av-mRFP/CyO* (Yokoshi *et al.*, 2020), *DSCP$_{WT}$-MS2-yellow-sna shadow enhancer* (Yokoshi *et al.*, 2020), *DSCP$_{mTATA}$-MS2-yellow-sna shadow enhancer* (this study), *DSCP$_{mInr}$-MS2-yellow-sna shadow enhancer* (this study), *DSCP$_{mMTE}$-MS2-yellow-sna shadow enhancer* (this study), *DSCP$_{mDPE}$-MS2-yellow-sna shadow enhancer* (this study), *DSCP$_{mGAGA}$-MS2-yellow-sna shadow enhancer* (this study), *DSCP$_{3xZelda}$-MS2-yellow-sna shadow enhancer* (this study), *DSCP$_{PB}$-MS2-yellow-sna shadow enhancer* (this study), *DSCP$_{mTATA/PB}$-MS2-yellow-sna shadow enhancer* (this study), *DSCP$_{WT}$-MS2-yellow-rhoNEE* (this study), *DSCP$_{mTATA}$-MS2-yellow-rhoNEE* (this study), *DSCP$_{mInr}$-MS2-yellow-rhoNEE* (this study), *DSCP$_{mMTE}$-MS2-yellow-rhoNEE* (this study), *DSCP$_{mDPE}$-MS2-yellow-rhoNEE* (this study), *Δftz-attP/TM6* (this study), *ftz WT core promoter-ftz-HA-24xMS2* (this study), *ftz mTATA core promoter-ftz-HA-24xMS2/TM6* (this study), and *ftz mDPE core promoter-ftz-HA-24xMS2/TM6* (this study).

Site specific transgenesis by phiC31 system

All reporter plasmids were integrated into a unique landing site on the third chromosome using VK00033 strain (Venken *et al.*, 2006). PhiC31 was maternally provided using vas-phiC31 strain (Bischof *et al*, 2007). Microinjection was performed as previously described (Ringrose, 2009). In brief, 0-1 h embryos were collected and dechorionated with bleach. Aligned embryos were dried with silica gel for ~7 min and covered with FL-100-1000CS silicone oil (Shin-Etsu Silicone). Subsequently, microinjection was performed using FemtoJet (Eppendorf) and DM IL LED inverted microscope (Leica) equipped with M-152 Micromanipulator (Narishige). Injection mixture typically contains ~500 ng/µl plasmid DNA, 5 mM KCl ,0.1 mM phosphate buffer, pH 6.8. mini-white marker was used for screening.

Core promoter modification at endogenous locus

First, endogenous *ftz* transcription unit was removed and replaced with attP site by CRISPR/Cas9-mediated genome editing. Two pCFD3 gRNA expression plasmids and pBS-attP-dsRed donor plasmid were co-injected using *nanos-Cas9/CyO* strain (Ren *et al*, 2013). Injection mixture contains 500 ng/µl pCFD3 gRNA expression plasmids, 500 ng/µl pBS-attP-dsRed donor plasmid, 5 mM KCl, 0.1 mM phosphate buffer, pH 6.8.

Resulting *ftz* allele were balanced over TM6. Subsequently, *ftz-MS2* plasmid was integrated into the attP site using *Δftz-attP/TM6* strain. Corresponding MS2 plasmid and p3x3-EGFP.vas-int.NLS plasmid (addgene #60948) were co-injected. Injection mixture contains 500 ng/μl MS2 plasmid, 500 ng/μl phiC31 expression plasmid, 5 mM KCl, 0.1 mM phosphate buffer, pH 6.8. mini-white marker was used for screening. Resulting *ftz* complementation alleles were balanced over TM6. After phiC31-mediated integration, extra sequences derived from plasmid backbone, ampicillin resistant gene and mini-white marker gene were also incorporated into the *ftz* locus.

cDNA synthesis

Total RNA was extracted from 40 adults of Oregon-R using TRIzol reagent (Thermo Fisher) followed by chloroform purification and isopropanol precipitation. Three μg of total RNA was subjected to reverse transcription using PrimeScript 1st strand cDNA Synthesis Kit (Takara).

Preparation of probes for *in situ* hybridization

Antisense RNA probes labeled with digoxigenin (DIG RNA Labeling Mix 10 × conc, Roche) and biotin (Biotin RNA Labeling Mix 10 × conc, Roche) were *in vitro* transcribed using *in vitro* Transcription T7 Kit (Takara). Template DNA for *ftz* probe was PCR amplified from genomic DNA using primers (5′-CGT AAT ACG ACT CAC TAT AGG GTG GGG AAG AGA GTA ACT GAG CAT CGC-3′) and (5′-ATT CGC AAA CTC ACC AGC GT-3′). Template DNA for *en* probe was PCR amplified from cDNA using primers (5′-CGT AAT ACG ACT CAC TAT AGG GCA TGA ACT TGC TTT AGC ACA AAC ATT TCG-3′) and (5′-CAA CTA ATT CAG TCG TTG CGC TCG-3′).

Fluorescence *in situ* hybridization

Embryos were dechorionated and fixed in fixation buffer (1 ml of 5x PBS, 4 ml of 37% formaldehyde and 5 ml of Heptane) for ~25 min at room temperature. Vitelline membrane was then removed by shaking embryos in a biphasic mixture of heptane and methanol for ~1 min. Antisense RNA probes labeled with digoxigenin and biotin were used. Hybridization was performed at 55℃ overnight in hybridization buffer (50% formamide, 5x SSC, 50 μg/ml Heparin, 100 μg/ml salmon sperm DNA, 0.1% Tween-20). Subsequently, embryos were washed with hybridization buffer at 55℃ and incubated with Western Blocking Reagent (Roche) at room temperature for one hour. Then, embryos were incubated with sheep anti-digoxigenin (Roche) and mouse anti-biotin primary antibodies (Invitrogen) at 4℃ for overnight, followed by incubation with Alexa Fluor 555

donkey anti-sheep (Invitrogen) and Alexa Flour 488 goat anti-mouse (Invitrogen) fluorescent secondary antibodies at room temperature for one hour. DNA was stained with DAPI, and embryos were mounted in ProLong Gold Antifade Mountant (Thermo Fisher Scientific). Imaging was performed on a Zeiss LSM 900 confocal microscope. Plan-Apochromat 20x / 0.8 N.A. objective was used. Images were captured in 16-bit. Maximum projections were obtained for all z-sections, and resulting images were shown. Brightness of images was linearly adjusted using Fiji (https://fiji.sc).

Western blot analysis

Two-four h embryos were collected and twice the volume of 2x SDS sample buffer was added. Subsequently, embryos were crushed with a pestle and boiled at 95℃ for 7 min. Insoluble pellet was removed by centrifugation and lysates were separated by SDS-PAGE, transferred to Immobilon-P PVDF membranes (Merck), and immunoblotted with antibodies. The primary antibodies used were as follows: rat monoclonal anti-HA High Affinity antibody (Roche, 1:1000), mouse monoclonal anti-α-Tubulin antibody (Sigma, 1:10000).

MS2 live imaging

Virgin females of *nanos>MCP-GFP, His2Av-mRFP/CyO* (Yokoshi et al., 2020) were mated with males carrying the MS2 allele. The resulting embryos were dechorionated and mounted between a polyethylene membrane (Ube Film) and a coverslip (18 mm x 18 mm), and embedded in FL-100-450CS (Shin-Etsu Silicone). Embryos were imaged using a Zeiss LSM 800 (Figure 1, EV3 and EV4) or LSM900 (Figure 2, 4 and EV2). Temperature was kept in between 23.5 to 25.0℃ during imaging. Plan-Apochromat 40x / 1.4 N.A. oil immersion objective was used. At each time point, a stack of 26 images separated by 0.5 μm was acquired. Typical time resolution of resulting maximum projection was 0.28 min. In subsequent image analysis, all movies were considered to have same time resolution (0.28 min/frame). Images were captured in 16-bit. Images were typically taken from the end of nc 13 to the onset of gastrulation at nc14. During imaging, data acquisition was occasionally stopped for a few seconds to correct z-position, and data were concatenated afterwards. For each cross, three biological replicates were taken. The same laser power and microscope setting were used for each set of experiments.

Quantification of hatching rate

In Figure 3F, 70 males and 70 virgin females were collected and mated in a cage with apple juice agar plate and yeast paste for 2 days at 25℃. After exchanging plates twice in

the morning, the eggs on the plates were collected within 3 hours. Five hundred eggs were placed on new apple juice agar plates and incubated at 25℃ for 2 days, followed by counting the number of hatched larvae. In Figure EV5B, virgin *yw* females were initially crossed with males of *Δftz-attP/TM6*, *ftz WT core promoter-ftz-HA-24xMS2*, *ftz mTATA core promoter-ftz-HA-24xMS2/TM6*, and *ftz mDPE core promoter-ftz-HA-24xMS2/TM6*. Hundred males and 100 virgin females of heterozygote mutants were collected from each cross, and mated in a cage with apple juice agar plate and yeast paste for 2 days at 25℃. After exchanging plates twice in the morning, the eggs on the plates were collected within 3 hours. Five hundred eggs were placed on new apple juice agar plates and incubated at 25℃ for 2 days, followed by counting the number of hatched larvae. Three independent experiments were performed to determine hatching rates.

ChIP-qPCR analysis

One-three h embryos were dechorionated and rinsed with water. They were crosslinked in a mixture of (2 ml of (1x PBS, 0.5% Triton X-100), 6 ml of heptane and 100 μl of 37% formaldehyde), followed by vigorous shaking for 10 min at room temperature. Subsequently, embryos were collected by centrifugation at 1,000 g for 1 min, and then added 5 ml of (1x PBS, 0.5% Triton X-100, 125 mM glycine), followed by vigorous shaking for 1 min at room temperature. Embryos were washed 3 times with 1x PBS, 0.5% Triton X-100. After removing whole supernatant, embryos were flash-frozen in liquid nitrogen and stored at -80℃. Upon thawing, 150-200 mg of embryos were resuspended in buffer A1 (15 mM HEPES pH 7.5, 15 mM NaCl, 60 mM KCl, 4 mM $MgCl_2$, 0.5% Triton X-100, 0.5 mM DTT, 1x protease inhibitor (Nacalai)) and homogenized 30 times on ice using a 7 ml dounce homogenizer (Wheaton). The homogenate was transferred to a 15 ml tube and centrifuged for 5 min at 15,000 g at 4℃. The pellet was resuspended in 2 ml buffer A1 by pipetting, and washed twice with buffer A1 and once with buffer A2 (15 mM HEPES pH 7.5, 140 mM NaCl, 1 mM EDTA, 0.5 mM EGTA, 1% Triton X-100, 0.1% sodium deoxycholate, 0.1% SDS, 0.5% N-lauroylsarcosine, 1x proteinase inhibitor (Nacalai)). Samples were added in 1 ml buffer A2 and sonicated on ice 8 times for 30 sec using UD-211 ultrasonic disrupter (TOMY, output control 3, duty cycle 10%), yielding the average size of chromatin fragments between 300-700 bp. Then, sonicated samples were centrifuged for 10 min at 15,000 g at 4℃, and supernatants were collected.

For immunoprecipitation, 20 μl of protein G magnetic beads (Invitrogen) were washed 3 times with (1x PBS, 0.5% BSA), and then pre-incubated with 2 μg antibodies (anti-RNA Pol II CTD4H8, Millipore; normal mouse IgG, Santa Cruz) in 500 μl of (1x PBS, 0.5%

BSA) at 4℃ for 8 hours on a rotating wheel. After washing twice with (1x PBS, 0.5% BSA) and once with buffer A2, magnetic beads were resuspended in 50 µl buffer A2. For each ChIP sample, 450 µl of the chromatin extract was incubated with 50 µl pre-mixed magnetic beads-antibody mixture overnight at 4℃ on a rotating wheel. For each sample, 45 µl (corresponding to 10 % of the ChIP sample volume) was set apart and stored at -80℃ for 10 % input genomic DNA for qPCR standard.

The next day, the beads were washed 4 times with ice-cold RIPA buffer (50 mM HEPES pH 7.5, 500 mM LiCl, 1 mM EDTA, 1% NP-40, 0.7% sodium deoxycholate) and then once with ice-cold TE50 buffer (50 mM Tris-HCl pH 8.0, 10 mM EDTA). After the last washing step, 100 µl of elution buffer (TE50 buffer, 1% SDS) was used to resuspend the beads, and immunoprecipitated samples were eluted at 65℃ for 40 min with vortexing every 5 min. Samples were centrifuged at 15,000 g and supernatants were transferred to fresh tubes. ChIP samples and input samples were adjusted to 100 µl with elution buffer and reverse crosslinked by incubating at 65℃ overnight. The following day, 100 µl TE buffer (10 mM Tris-HCl pH 8.0, 1 mM EDTA) and 0.1 µl of 20 mg/ml RNaseA (Sigma) were added (final concentration 10 µg/ml) and incubated at 37℃ for 1 hour, and then treated with 2 µl of 350 U/ml protease K (Takara) at 55℃ for 2 hours. The volume of samples was adjusted to 400 µl with TE buffer, and purified with an equal volume of phenol/chloroform/isoamyl alcohol (25:24:1). After centrifugation at 15,000 g for 5 min at room temperature, supernatants (320 µl) were transferred to a new tube. DNA was precipitated by addition of 2 µl of 20 mg/ml glycogen, 32 µl of 3 M sodium acetate and 560 µl of -30℃ 100% ethanol. The samples were then incubated for 1 hour at -30℃ and centrifuged at 15,000 g for 10 min at 4℃. Finally, DNA pellets were washed twice with 800 µl of -30℃ 80% ethanol and resuspended in 20 µl water. Three independent chromatin preparations were made for each ChIP samples.

qPCR was performed using KAPA SYBR FAST qPCR Master mix (Kapa Biosystems) in LightCycler 480 II (Roche). The qPCR reactions were run using the following program: pre-incubation for 3 min at 95℃ followed by 40 cycles of (initial denaturation for 10 sec at 95℃, annealing for 20 sec at 60℃ and extension for 1 sec at 72℃). 1 µl of sample DNA was used for each PCR reaction in a total volume of 20 µl. Primers (5′-TGT GAA TGA ATG TTC GAG CCG AGC-3′) and (5′-AGG ATC CGT TTG GTA TGC GTC-3′) were used for the measurement of Pol II occupancy at the core promoter region. Primers (5′-CCC ATC TAT TTC CCA CCC ATC AAC C-3′) and (5′-ACG CTT AGT GGC GCG CCT TAA C-3′) were used for the measurement of Pol II occupancy at the gene body. All

reactions were performed in technical triplicate. Threshold cycle (Ct) values were determined by manual thresholding using the LightCycler 480 software (Roche). A pausing index was defined by percentage of input of the core promoter region divided by percentage of input of the gene body.

Plasmids

pbphi-DSCP$_{mTATA}$-MS2-yellow-sna shadow enhancer

Two DNA oligos (5′-TTT CCC TCG AGG AGC TCG CCC GGG GAT CGA GCG CAG CGG GCG CCC CGG GCG CGG GGT GGC TGA GAG CAT CAG TTG TGA ATG AAT GTT CGA GCC GAG C-3′) and (5′-GGA AAG GAT CCG TTT GGT ATG CGT CTT GTG ATT CAA AGT TGG CTT ATT CAA AGG ATA TTA ACG AAG GCA GCG GCA CGT CTG CTC GGC TCG AAC AT-3′) were annealed and blunt-ended by PCR. Resulting DNA fragment was inserted between XhoI and BamHI sites of pbphi-DSCP-MS2-yellow (Yokoshi *et al.*, 2020). Subsequently, a DNA fragment containing *sna* shadow enhancer was purified from pbphi-snail shadow enhancer (Lim *et al*, 2018) by digesting with HindIII and NheI. The resulting fragment was inserted between the HindIII and NheI sites of the plasmid.

pbphi-DSCP$_{mInr}$-MS2-yellow-sna shadow enhancer

Two DNA oligos (5′-TTT CCC TCG AGG AGC TCG CCC GGG GAT CGA GCG CAG CGG TAT AAA AGG GCG CGG GGT GGC TGA GAG CAG TGA CAG TGA ATG AAT GTT CGA GCC GAG C-3′) and (5′-GGA AAG GAT CCG TTT GGT ATG CGT CTT GTG ATT CAA AGT TGG CTT ATT CAA AGG ATA TTA ACG AAG GCA GCG GCA CGT CTG CTC GGC TCG AAC AT-3′) were annealed and blunt-ended by PCR. Resulting DNA fragment was inserted between XhoI and BamHI sites of pbphi-DSCP-MS2-yellow (Yokoshi *et al.*, 2020). Subsequently, a DNA fragment containing *sna* shadow enhancer was inserted between HindIII and NheI sites of the plasmid.

pbphi-DSCP$_{mMTE}$-MS2-yellow-sna shadow enhancer

Two DNA oligos (5′-TTT CCC TCG AGG AGC TCG CCC GGG GAT CGA GCG CAG CGG TAT AAA AGG GCG CGG GGT GGC TGA GAG CAT CAG TTG TGA ATG AAT GTT ATC CAC GAG C-3′) and (5′-GGA AAG GAT CCG TTT GGT ATG CGT CTT GTG ATT CAA AGT TGG CTT ATT CAA AGG ATA TTA ACG AAG GCA GCG GCA CGT CTG CTC GTG GAT AAC AT-3′) were annealed and blunt-ended by PCR. Resulting DNA fragment was inserted between XhoI and BamHI sites of pbphi-DSCP-MS2-yellow (Yokoshi *et al.*, 2020). Subsequently, a DNA fragment containing *sna*

shadow enhancer was inserted between HindIII and NheI sites of the plasmid.

pbphi-DSCP$_{mDPE}$-MS2-yellow-sna shadow enhancer

Two DNA oligos (5′-TTA AAC TCG AGG AGC TCG CCC GGG GAT CGA GCG CAG CGG TAT AAA AGG GCG CGG GGT GGC TGA GAG CAT CAG TTG TGA ATG AAT GTT CGA GCC GAG C-3′) and (5′-ACA TGG GAT CCG TTT GGT ATG CGT CTT GTG ATT CAA AGT TGG CTT ATT CAA AGG ATA TTA ACG AAG GCA GCG GCC ATG AGG CTC GGC TCG AAC ATT CAT T-3′) were annealed and blunt-ended by PCR. Resulting DNA fragment was inserted between XhoI and BamHI sites of pbphi-DSCP-MS2-yellow (Yokoshi *et al.*, 2020). Subsequently, a DNA fragment containing *sna* shadow enhancer was inserted between HindIII and NheI sites of the plasmid.

pbphi-DSCP$_{mGAGA}$-MS2-yellow-sna shadow enhancer

Two DNA oligos (5′-TTA AAC TCG AGG AGC TCG CCC GGG GAT CGA GCG CAG CGG TAT AAA AGG GCG CGG GGT GGC TCA CTG CAT CAG TTG TGA ATG AAT GTT CGA GCC GAG C-3′) and (5′-ACA TGG GAT CCG TTT GGT ATG CGT CTT GTG ATT CAA AGT TGG CTT ATT CAA AGG ATA TTA ACG AAG GCA GCG GCA CGT CTG CTC GGC TCG AAC ATT CAT T-3′) were annealed and blunt-ended by PCR. Resulting DNA fragment was inserted between XhoI and BamHI sites of pbphi-DSCP-MS2-yellow (Yokoshi *et al.*, 2020). Subsequently, a DNA fragment containing *sna* shadow enhancer was inserted between HindIII and NheI sites of the plasmid.

pbphi-DSCP$_{3xZelda}$-MS2-yellow-sna shadow enhancer

Two DNA oligos (5′-TTT CCC TCG AGC AGG TAG CCC GGG GAT CGA GCG CAG CGG TAT AAA AGG GCG CGG GGT GGC TGA GAG CAT CAG TTG TGA ATG AAT GTT CGA GCC GAG C-3′) and (5′-GGA AAG GAT CCG TTT GGT ATG CGT CTT GTG ATT CAA AGT TGG CTT ATT CAA AGG ATA TTA ACG AAG GCA GCG GCA CGT CTG CTC GGC TCG AAC AT-3′) were annealed and blunt-ended by PCR. Resulting DNA fragment was inserted between XhoI and BamHI sites of pbphi-DSCP-MS2-yellow (Yokoshi *et al.*, 2020). Subsequently, two DNA oligos (5′-GGC CGC CAG GTA GCA GGT AGC-3′) and (5′-TCG AGC TAC CTG CTA CCT GGC-3′) were annealed and inserted into the plasmid using NotI and XhoI sites. Then, a DNA fragment containing *sna* shadow enhancer was inserted between HindIII and NheI sites of the plasmid.

pbphi-DSCP$_{PB}$-MS2-yellow-sna shadow enhancer

Two DNA oligos (5′-TTT CCC TCG AGG AGC TCG CCC GGG GAT CGA GCG CAG CGG TAT AAA AGG GCG CGG GGT GGC TGA GAG CAT CAG TTG TGA ATG AAT GTT CGA GCC GAG C-3′) and (5′-GGA AAG GAT CCG TTT GGT ATG CGT CTT GTG ATT CAA AGT TGG CTT ATT CAA AGG ATA TTA ACG AAG GCA GCG GCA CGT CCG CTC GGC TCG AAC AT-3′) were annealed and blunt-ended by PCR. Resulting DNA fragment was inserted between XhoI and BamHI sites of pbphi-DSCP-MS2-yellow (Yokoshi *et al.*, 2020). Subsequently, a DNA fragment containing *sna* shadow enhancer was inserted between HindIII and NheI sites of the plasmid.

pbphi-DSCP$_{mTATA/PB}$-MS2-yellow-sna shadow enhancer

Two DNA oligos (5′-TTA AAG CGG CCG CGG GAA TTC GAT TCT CGA GGA GCT CGC CCG GGG ATC GAG CGC AGC GGG CGC CCC GGG CGC GGG GTG GCT GAG AGC ATC AGT TGT GAA TGA ATG TTC GAG CCG AGC-3′) and (5′-ACA TGG GAT CCG TTT GGT ATG CGT CTT GTG ATT CAA AGT TGG CTT ATT CAA AGG ATA TTA ACG AAG GCA GCG GCA CGT CCG CTC GGC TCG AAC ATT CAT T-3′) were annealed and blunt-ended by PCR. Resulting DNA fragment was inserted between NotI and BamHI sites of pbphi-DSCP-MS2-yellow-*sna* shadow enhancer (Yokoshi *et al.*, 2020).

pbphi-DSCP$_{WT}$-MS2-yellow-rhoNEE

A DNA fragment containing *rho*NEE was inserted between the HindIII and NheI sites of pbphi-DSCP$_{WT}$-MS2-yellow-sna shadow enhancer. Sequence of *rho*NEE is the same as one used in the previous study (Fukaya *et al.*, 2016).

pbphi-DSCP$_{mTATA}$-MS2-yellow-rhoNEE

A DNA fragment containing *rho*NEE was inserted between the HindIII and NheI sites of pbphi-DSCP$_{mTATA}$-MS2-yellow-sna shadow enhancer. Sequence of *rho*NEE is the same as one used in the previous study (Fukaya *et al.*, 2016).

pbphi-DSCP$_{mInr}$-MS2-yellow-rhoNEE

A DNA fragment containing *rho*NEE was inserted between the HindIII and NheI sites of pbphi-DSCP$_{mInr}$-MS2-yellow-sna shadow enhancer. Sequence of *rho*NEE is the same as one used in the previous study (Fukaya *et al.*, 2016).

pbphi-DSCP$_{mMTE}$-MS2-yellow-rhoNEE

A DNA fragment containing *rho*NEE was inserted between the HindIII and NheI sites of

pbphi-DSCP$_{mMTE}$-MS2-yellow-sna shadow enhancer. Sequence of *rho*NEE is the same as one used in the previous study (Fukaya *et al.*, 2016).

pbphi-DSCP$_{mDPE}$-MS2-yellow- rhoNEE

A DNA fragment containing *rho*NEE was inserted between the HindIII and NheI sites of pbphi-DSCP$_{mDPE}$-MS2-yellow-sna shadow enhancer. Sequence of *rho*NEE is the same as one used in the previous study (Fukaya *et al.*, 2016).

pBS-attP-dsRed-SV40

Two DNA oligos (5′-TCG ACA GTT CTA GAC CCC CAA CTG AGA GAA CTC AAA GGT TAC CCC AGT TGG GGG AAT TCA TCG ATA ACT TCG TAT AAT GTA TGC TAT ACG AAG TTA TG-3′) and (5′-CTA GCA TAA CTT CGT ATA GCA TAC ATT ATA CGA AGT TAT CGA TGA ATT CCC CCA ACT GGG GTA ACC TTT GAG TTC TCT CAG TTG GGG GTC TAG AAC TG-3′) were annealed and inserted into the modified version of pBS-3xP3-dsRed plasmid using SalI and NheI sites.

pCFD3-dU6-ftz-1

Two DNA oligos (5′-GTC GCT GCA AGG ACA TTT CGC CGG-3′) and (5′-AAA CCC GGC GAA ATG TCC TTG CAG-3′) were annealed and inserted into the pCFD3-dU6:3gRNA vector (addgene # 49410) using BbsI sites.

pCFD3-dU6-ftz-2

Two DNA oligos (5′-GTC GCA ATT TGT GAA GAA GAG TCT-3′) and (5′-AAA CAG ACT CTT CTT CAC AAA TTG-3′) were annealed and inserted into the pCFD3-dU6:3gRNA vector (addgene # 49410) using BbsI sites.

pBS-ftz 5′Arm-attP-dsRed-SV40-ftz 3′Arm

A DNA fragment containing 3′ homology arm of *ftz* was amplified from genomic DNA using primers (5′-TTT AAA CTA GTT CTT GGG CAT GCT GCA ATT TG-3′) and (5′-TTA AAG CGG CCG CGA AGG GTA GGA TAG AAT CTG-3′), and digested with SpeI and NotI. The resulting fragment was inserted between the SpeI and NotI sites of pBS-attP-dsRed-SV40. Subsequently, a DNA fragment containing 5′ homology arm of *ftz* was amplified from genomic DNA using primers (5′-TTT AAG GTA CCA TGA AGA TCC TAC GCT GTG C-3′) and (5′-TTA AAG TCG ACG CGA AAT GTC CTT GCA GGC ACG-3′), and digested with KpnI and SalI. The resulting fragment was inserted between the KpnI and SalI sites of the plasmid.

pbphi-ftz WT core promoter-ftz-HA-24xMS2-aTub 3′UTR

A DNA fragment containing *ftz* transcription unit fused with C-terminal HA-tag was amplified from genomic DNA using primers (5′-TTT AAG GAT CCA CTA GTA TGG CCA CCA CAA ACA GCC AGA GC-3′) and (5′-TTA AAG GAT CCT CAT GCA TAA TCC GGA ACA TCA TAC GGA TAA GAC AGA TGG TAG AGG TCC TGT GG-3′), and digested with BamHI. The resulting fragment was inserted between the BglII and BamHI sites of the pbphi-hbP2 promoter-lacZ-24xMS2-αTub 3′UTR (modified version of pbphi-hbP2 promoter-lacZ-24xPP7-αTub 3′UTR described in (Fukaya *et al*, 2017)). Subsequently, a DNA fragment containing native *ftz* core promoter sequence was amplified from genomic DNA using primers (5′-TTT AAA AGC TTT GTC ATG CGC AGG GAT ATT TAT GCG-3′) and (5′-TTA AAA CTA GTA TCG GAT GTG TAT TGC TAG ATT TC-3′), and digested with HindIII and SpeI. The resulting fragment was inserted between the HindIII and SpeI sites of the plasmid.

pbphi-ftz mTATA core promoter-ftz-HA-24xMS2-aTub 3′UTR

Two DNA oligos (5′-ACT ATA AGC TTT GTC ATG CGC AGG GAT ATT TAT GCG CTA TAA CGC CGA GCG TGT GCC GAG GGC TCT CTG ATT TTG CGC GCC CCG CAG GAT CTG CCG CAG G-3′) and (5′-AAT CCA CTA GTA TCG GAT GTG TAT TGC TAG ATT TCT TCT CTA ACT CTG CGA TGT GCA CGC AAC GCT GGT GAG TTT GCG AAT GAG CTG GTC CTG CGG CAG ATC CTG CGG G-3′) were annealed and blunt-ended by PCR. The resulting fragment was inserted between the HindIII and SpeI sites of pbphi-ftz WT core promoter-ftz-HA-24xMS2-aTub 3′UTR.

pbphi-ftz mDPE core promoter-ftz-HA-24xMS2-aTub 3′UTR

Two DNA oligos (5′-ACA TGA AGC TTT GTC ATG CGC AGG GAT ATT TAT GCG CTA TAA CGC CGA GCG TGT GCC GAG GGC TCT CTG ATT TTG CTA TAT ATG CAG GAT CTG CCG CAG G-3′) and (5′-AAT CCA CTA GTA TCG GAT GTG TAT TGC TAG ATT TCT TCT CTA ACT CTG CAT GAG GCA CGC AAC GCT GGT GAG TTT GCG AAT GAG CTG GTC CTG CGG CAG ATC CTG CAT A-3′) were annealed and blunt-ended by PCR. The resulting fragment was inserted between the HindIII and SpeI sites of pbphi-ftz WT core promoter-ftz-HA-24xMS2-aTub 3′UTR.

Image analysis

All the image processing methods and analysis were implemented in MATLAB (R2019b, MathWorks).

Segmentation of nuclei

For each time point, maximum projections were obtained for all 26 z-sections per image. His2Av-mRFP was used to segment nuclei. 512 x 512 maximum projection images were initially cropped into 430 x 430 (Figure 1, 4, EV3 and EV4) or 300 x 430 (Figure 2) to remove nuclei at the edge, and used for subsequent analysis. In the analysis of *rho*NEE reporters (Figure EV2), 512 x 512 maximum projection images were initially cropped into 300 x 500 to remove nuclei outside of the expression domain. For nuclei segmentation, we used two different methods. In the first method, His2Av images were pre-processed with Gaussian filtering, top-hap filtering, and adaptive histogram equalization, in order to enhance the signal-to-noise contrast. Processed images were converted into binary images using a threshold value obtained from Otsu's method. Nuclei were then watershedded to further separate and distinguish from neighboring nuclei. Subsequently, binary images were manually corrected using Fiji (https://fiji.sc). In the second method, His2Av images were first blurred with Gaussian filter to generate smooth images. Pixels expressing intensity higher than 5% of the global maxima in the histogram of His2Av channel were removed. Processed images were converted into binary images using a custom threshold-adaptative segmentation algorithm. Threshold values were determined at each time frame by taking account of 1) histogram distribution of His2Av channel and 2) the number and size of resulting connected components. Boundaries of components were then modified to locate MS2 transcription dots inside of nearest nuclei. In brief, pixels with intensity twice larger than mean intensity of MS2 channel were considered as transcription dots, and new binary images were created for each time frame. The Euclidean distances between the centroid of binarized transcription dot and all boundaries of segmented nuclei were calculated. Boundary of the nucleus with the smallest Euclidean distance was modified in order to capture transcription dot within a nucleus. Centroids of connected components in nuclei segmentation channel were used to compute the Voronoi cells of the image. Resulting binary images were manually corrected by using Fiji (https://fiji.sc).

Tracking of nuclei

Nuclei tracking was done by finding the object with minimal movement across the frames of interest. For each nucleus in a given frame, the Euclidean distances between the centroids of the nucleus in current time frame and the nuclei in the next or previous time frame were determined. The nucleus with the minimum Euclidean distance was considered as the same lineage.

Recording of MS2 signals

Maximum projections of raw images were used to record MS2 fluorescence intensities. Using segmented regions, fluorescence intensities within each nucleus were extracted. Signals of MS2 transcription dots were determined by taking an average of the top three pixels with the highest fluorescence intensity within each nucleus. After obtaining MS2 trajectories, median fluorescence intensities within a nucleus were subtracted as a background. In Figure EV2, signals of MS2 transcription dots were determined by taking integral in a 5 x 5 pixel region centering the brightest pixel within a nucleus after subtracting median fluorescence intensity within a nucleus as a background. Subsequently, minimum MS2 intensities were determined for individual trajectories and subtracted to make the baseline zero.

Detection of transcriptional bursting

A transcriptional burst was defined as a local change in fluorescence intensity. First, signal trajectories were smoothed by the moving average method. When a nucleus had above-threshold transcription activity, burst was considered to be started. Burst was considered to be ended when the intensity dropped below 55% of the local peak value. When the burst duration is less than 5 timeframes, it was considered as a false-positive derived from detection noise. When signal trace exhibited continuous decreasing at the beginning of burst detection, it was also not considered as a burst. Location of defined burst was then moved two timeframes afterwards to better capture the center of individual bursting event. Same method and threshold value were used for each set of experiments.

Description of bursting properties

From each trajectory, number of bursts, amplitude and duration of each burst, and total integrated signal (output) produced by each nucleus were measured. To determine amplitude, the peak value during the burst was measured using trajectories after smoothing. The duration was determined by measuring the length of each burst. Total RNA production was measured by taking the area under the raw trajectory. The amplitude and duration for each nucleus were determined by taking average of all analyzed bursts in a single nucleus.

Fraction of instantaneously active nuclei

For each time frame, nuclei with MS2 intensity above the threshold were considered as active. Threshold was determined for each group by calculating the 10% of the maximum MS2 intensity across all trajectories within a group.

Mean MS2 intensity per actively transcribing nucleus

MS2 intensities in instantaneously active nuclei at each time point were averaged.

Computational reconstitution of *ftz* expression

Newly synthesized *ftz* mRNAs were considered to be linearly degraded with a half-life of 7 min according to previous measurements in early embryos (Edgar *et al.*, 1986). Amount of *ftz* mRNA remained to be undegraded at the end of analysis was estimated using live imaging data. Using segmentation mask, individual nuclei were false-colored with the pixel intensity proportional to the level of intact *ftz* mRNA in a given nucleus. Resulting image was then colored and layered over the maximum projected image of His2Av-mRFP.

False-coloring by instantaneous MS2 signals

MS2 signal intensity at each nucleus was measured as described in the previous section. Using segmentation mask, individual nuclei were false-colored with the pixel intensity proportional to the instantaneous MS2 signal at given time in a given nucleus. Resulting image was then colored and layered over the maximum projected image of His2Av-mRFP.

References

Bartman CR, Hsu SC, Hsiung CC, Raj A, Blobel GA (2016) Enhancer Regulation of Transcriptional Bursting Parameters Revealed by Forced Chromatin Looping. *Mol Cell* 62: 237-247

Bertrand E, Chartrand P, Schaefer M, Shenoy SM, Singer RH, Long RM (1998) Localization of ASH1 mRNA particles in living yeast. *Mol Cell* 2: 437-445

Bischof J, Maeda RK, Hediger M, Karch F, Basler K (2007) An optimized transgenesis system for *Drosophila* using germ-line-specific phiC31 integrases. *P Natl Acad Sci USA* 104: 3312-3317

Bothma JP, Garcia HG, Esposito E, Schlissel G, Gregor T, Levine M (2014) Dynamic regulation of *eve* stripe 2 expression reveals transcriptional bursts in living *Drosophila* embryos. *Proc Natl Acad Sci U S A* 111: 10598-10603

Burke TW, Kadonaga JT (1996) Drosophila TFIID binds to a conserved downstream basal promoter element that is present in many TATA-box-deficient promoters. *Genes Dev* 10: 711-724

Burke TW, Kadonaga JT (1997) The downstream core promoter element, DPE, is conserved from *Drosophila* to humans and is recognized by TAFII60 of *Drosophila*. *Genes Dev* 11: 3020-3031

Butler JE, Kadonaga JT (2001) Enhancer-promoter specificity mediated by DPE or TATA core promoter motifs. *Genes Dev* 15: 2515-2519

Calhoun VC, Levine M (2003) Long-range enhancer-promoter interactions in the *Scr-Antp* interval of the *Drosophila* Antennapedia complex. *Proc Natl Acad Sci U S A* 100: 9878-9883

Carroll SB, Scott MP (1986) Zygotically active genes that affect the spatial expression of the *fushi tarazu* segmentation gene during early *Drosophila* embryogenesis. *Cell* 45: 113-126

Chalkley GE, Verrijzer CP (1999) DNA binding site selection by RNA polymerase II TAFs: a TAF(II)250-TAF(II)150 complex recognizes the initiator. *EMBO J* 18: 4835-4845

Chen K, Johnston J, Shao W, Meier S, Staber C, Zeitlinger J (2013) A global change in RNA polymerase II pausing during the *Drosophila* midblastula transition. *Elife* 2: e00861

Chen ZX, Sturgill D, Qu J, Jiang H, Park S, Boley N, Suzuki AM, Fletcher AR, Plachetzki DC, FitzGerald PC *et al* (2014) Comparative validation of the *D. melanogaster* modENCODE transcriptome annotation. *Genome Res* 24: 1209-1223

Chong S, Chen C, Ge H, Xie XS (2014) Mechanism of transcriptional bursting in bacteria. *Cell* 158: 314-326

Chubb JR, Trcek T, Shenoy SM, Singer RH (2006) Transcriptional pulsing of a developmental gene. *Curr Biol* 16: 1018-1025

Cianfrocco MA, Kassavetis GA, Grob P, Fang J, Juven-Gershon T, Kadonaga JT, Nogales E (2013) Human TFIID binds to core promoter DNA in a reorganized structural state. *Cell* 152: 120-131

Crocker J, Abe N, Rinaldi L, McGregor AP, Frankel N, Wang S, Alsawadi A, Valenti P, Plaza S, Payre F *et al* (2015) Low affinity binding site clusters confer hox specificity and regulatory robustness. *Cell* 160: 191-203

DiNardo S, O'Farrell PH (1987) Establishment and refinement of segmental pattern in the *Drosophila* embryo: spatial control of *engrailed* expression by pair-rule genes. *Genes Dev* 1: 1212-1225

Dunipace L, Ozdemir A, Stathopoulos A (2011) Complex interactions between cis-regulatory modules in native conformation are critical for *Drosophila snail* expression. *Development* 138: 4075-4084

Edgar BA, Weir MP, Schubiger G, Kornberg T (1986) Repression and turnover pattern *fushi tarazu* RNA in the early *Drosophila* embryo. *Cell* 47: 747-754

Farley EK, Olson KM, Zhang W, Brandt AJ, Rokhsar DS, Levine MS (2015) Suboptimization of developmental enhancers. *Science* 350: 325-328

FitzGerald PC, Sturgill D, Shyakhtenko A, Oliver B, Vinson C (2006) Comparative genomics of *Drosophila* and human core promoters. *Genome Biol* 7: R53

Frasch M, Levine M (1987) Complementary patterns of *even-skipped* and *fushi tarazu* expression involve their differential regulation by a common set of segmentation genes in *Drosophila*. *Genes Dev* 1: 981-995

Fuda NJ, Guertin MJ, Sharma S, Danko CG, Martins AL, Siepel A, Lis JT (2015) GAGA factor maintains nucleosome-free regions and has a role in RNA polymerase II recruitment to promoters. *PLoS Genet* 11: e1005108

Fukaya T, Lim B, Levine M (2016) Enhancer Control of Transcriptional Bursting. *Cell* 166: 358-368

Fukaya T, Lim B, Levine M (2017) Rapid Rates of Pol II Elongation in the *Drosophila* Embryo. *Curr Biol* 27: 1387-1391

Gaertner B, Johnston J, Chen K, Wallaschek N, Paulson A, Garruss AS, Gaudenz K, De Kumar B, Krumlauf R, Zeitlinger J (2012) Poised RNA polymerase II changes over developmental time and prepares genes for future expression. *Cell Rep* 2: 1670-1683

Garcia HG, Tikhonov M, Lin A, Gregor T (2013) Quantitative imaging of transcription

in living *Drosophila* embryos links polymerase activity to patterning. *Curr Biol* 23: 2140-2145

Goldberg ML (1979) Sequence analysis of *Drosophila* histone genes. *PhD Dissertation, Stanford University, Stanford, CA*

Groth AC, Fish M, Nusse R, Calos MP (2004) Construction of transgenic *Drosophila* by using the site-specific integrase from phage phiC31. *Genetics* 166: 1775-1782

Hafen E, Kuroiwa A, Gehring WJ (1984) Spatial distribution of transcripts from the segmentation gene *fushi tarazu* during *Drosophila* embryonic development. *Cell* 37: 833-841

Harrison MM, Li XY, Kaplan T, Botchan MR, Eisen MB (2011) Zelda binding in the early *Drosophila melanogaster* embryo marks regions subsequently activated at the maternal-to-zygotic transition. *PLoS Genet* 7: e1002266

Hendrix DA, Hong JW, Zeitlinger J, Rokhsar DS, Levine MS (2008) Promoter elements associated with RNA Pol II stalling in the *Drosophila* embryo. *Proc Natl Acad Sci U S A* 105: 7762-7767

Hiromi Y, Gehring WJ (1987) Regulation and function of the *Drosophila* segmentation gene *fushi tarazu*. *Cell* 50: 963-974

Hiromi Y, Kuroiwa A, Gehring WJ (1985) Control elements of the *Drosophila* segmentation gene *fushi tarazu*. *Cell* 43: 603-613

Howard K, Ingham P (1986) Regulatory interactions between the segmentation genes *fushi tarazu*, *hairy*, and *engrailed* in the *Drosophila* blastoderm. *Cell* 44: 949-957

Ip YT, Park RE, Kosman D, Bier E, Levine M (1992) The dorsal gradient morphogen regulates stripes of *rhomboid* expression in the presumptive neuroectoderm of the *Drosophila* embryo. *Genes Dev* 6: 1728-1739

Juven-Gershon T, Hsu JY, Kadonaga JT (2008) Caudal, a key developmental regulator, is a DPE-specific transcriptional factor. *Genes Dev* 22: 2823-2830

Kuroiwa A, Hafen E, Gehring WJ (1984) Cloning and transcriptional analysis of the segmentation gene *fushi tarazu* of *Drosophila*. *Cell* 37: 825-831

Kutach AK, Kadonaga JT (2000) The downstream promoter element DPE appears to be as widely used as the TATA box in *Drosophila* core promoters. *Mol Cell Biol* 20: 4754-4764

Larson DR, Zenklusen D, Wu B, Chao JA, Singer RH (2011) Real-time observation of transcription initiation and elongation on an endogenous yeast gene. *Science* 332: 475-478

Larsson AJM, Johnsson P, Hagemann-Jensen M, Hartmanis L, Faridani OR, Reinius B, Segerstolpe A, Rivera CM, Ren B, Sandberg R (2019) Genomic encoding of

transcriptional burst kinetics. *Nature* 565: 251-254

Lee C, Li X, Hechmer A, Eisen M, Biggin MD, Venters BJ, Jiang C, Li J, Pugh BF, Gilmour DS (2008) NELF and GAGA factor are linked to promoter-proximal pausing at many genes in *Drosophila*. *Mol Cell Biol* 28: 3290-3300

Lee C, Shin H, Kimble J (2019) Dynamics of Notch-Dependent Transcriptional Bursting in Its Native Context. *Dev Cell* 50: 426-435 e424

Lim B, Heist T, Levine M, Fukaya T (2018) Visualization of Transvection in Living *Drosophila* Embryos. *Mol Cell* 70: 287-296 e286

Lim CY, Santoso B, Boulay T, Dong E, Ohler U, Kadonaga JT (2004) The MTE, a new core promoter element for transcription by RNA polymerase II. *Genes Dev* 18: 1606-1617

Little SC, Tikhonov M, Gregor T (2013) Precise developmental gene expression arises from globally stochastic transcriptional activity. *Cell* 154: 789-800

Louder RK, He Y, Lopez-Blanco JR, Fang J, Chacon P, Nogales E (2016) Structure of promoter-bound TFIID and model of human pre-initiation complex assembly. *Nature* 531: 604-609

Lucas T, Ferraro T, Roelens B, De Las Heras Chanes J, Walczak AM, Coppey M, Dostatni N (2013) Live imaging of bicoid-dependent transcription in *Drosophila* embryos. *Curr Biol* 23: 2135-2139

Macdonald PM, Struhl G (1986) A molecular gradient in early *Drosophila* embryos and its role in specifying the body pattern. *Nature* 324: 537-545

McKnight SL, Miller OL, Jr. (1979) Post-replicative nonribosomal transcription units in *D. melanogaster* embryos. *Cell* 17: 551-563

Molina N, Suter DM, Cannavo R, Zoller B, Gotic I, Naef F (2013) Stimulus-induced modulation of transcriptional bursting in a single mammalian gene. *Proc Natl Acad Sci U S A* 110: 20563-20568

Nicolas D, Zoller B, Suter DM, Naef F (2018) Modulation of transcriptional burst frequency by histone acetylation. *Proc Natl Acad Sci U S A* 115: 7153-7158

Nüsslein-Volhard C, Frohnhofer HG, Lehmann R (1987) Determination of anteroposterior polarity in *Drosophila*. *Science* 238: 1675-1681

Nüsslein-Volhard C, Wieschaus, E., Jürgens, G. (1982) Segmentierung bei *Drosophila* — eine genetische Analyse. *Verh Ges Dtsch Zool*: 91-104

Ohler U, Liao GC, Niemann H, Rubin GM (2002) Computational analysis of core promoters in the *Drosophila* genome. *Genome Biol* 3: RESEARCH0087

Ohtsuki S, Levine M (1998) GAGA mediates the enhancer blocking activity of the eve promoter in the *Drosophila* embryo. *Genes Dev* 12: 3325-3330

Ohtsuki S, Levine M, Cai HN (1998) Different core promoters possess distinct regulatory activities in the *Drosophila* embryo. *Genes Dev* 12: 547-556

Pare A, Lemons D, Kosman D, Beaver W, Freund Y, McGinnis W (2009) Visualization of individual *Scr* mRNAs during *Drosophila* embryogenesis yields evidence for transcriptional bursting. *Curr Biol* 19: 2037-2042

Patel AB, Louder RK, Greber BJ, Grunberg S, Luo J, Fang J, Liu Y, Ranish J, Hahn S, Nogales E (2018) Structure of human TFIID and mechanism of TBP loading onto promoter DNA. *Science* 362

Perry MW, Boettiger AN, Bothma JP, Levine M (2010) Shadow enhancers foster robustness of *Drosophila* gastrulation. *Curr Biol* 20: 1562-1567

Pfeiffer BD, Jenett A, Hammonds AS, Ngo TT, Misra S, Murphy C, Scully A, Carlson JW, Wan KH, Laverty TR *et al* (2008) Tools for neuroanatomy and neurogenetics in *Drosophila*. *Proc Natl Acad Sci U S A* 105: 9715-9720

Pick L, Schier A, Affolter M, Schmidt-Glenewinkel T, Gehring WJ (1990) Analysis of the *ftz* upstream element: germ layer-specific enhancers are independently autoregulated. *Genes Dev* 4: 1224-1239

Raj A, Peskin CS, Tranchina D, Vargas DY, Tyagi S (2006) Stochastic mRNA synthesis in mammalian cells. *PLoS Biol* 4: e309

Ren XJ, Sun J, Housden BE, Hu YH, Roesel C, Lin SL, Liu LP, Yang ZH, Mao DC, Sun LZ *et al* (2013) Optimized gene editing technology for *Drosophila melanogaster* using germ line-specific Cas9. *P Natl Acad Sci USA* 110: 19012-19017

Ringrose L (2009) Transgenesis in *Drosophila* melanogaster. *Methods Mol Biol* 561: 3-19

Rodriguez J, Ren G, Day CR, Zhao K, Chow CC, Larson DR (2019) Intrinsic Dynamics of a Human Gene Reveal the Basis of Expression Heterogeneity. *Cell* 176: 213-226 e218

Schroeder MD, Greer C, Gaul U (2011) How to make stripes: deciphering the transition from non-periodic to periodic patterns in *Drosophila* segmentation. *Development* 138: 3067-3078

Shao W, Alcantara SG, Zeitlinger J (2019) Reporter-ChIP-nexus reveals strong contribution of the *Drosophila* initiator sequence to RNA polymerase pausing. *Elife* 8

Smale ST, Baltimore D (1989) The "initiator" as a transcription control element. *Cell* 57: 103-113

Sun Y, Nien CY, Chen K, Liu HY, Johnston J, Zeitlinger J, Rushlow C (2015) Zelda overcomes the high intrinsic nucleosome barrier at enhancers during *Drosophila*

zygotic genome activation. *Genome Res* 25: 1703-1714

Suter DM, Molina N, Gatfield D, Schneider K, Schibler U, Naef F (2011) Mammalian genes are transcribed with widely different bursting kinetics. *Science* 332: 472-474

Tantale K, Mueller F, Kozulic-Pirher A, Lesne A, Victor JM, Robert MC, Capozi S, Chouaib R, Backer V, Mateos-Langerak J *et al* (2016) A single-molecule view of transcription reveals convoys of RNA polymerases and multi-scale bursting. *Nat Commun* 7: 12248

Theisen JW, Lim CY, Kadonaga JT (2010) Three key subregions contribute to the function of the downstream RNA polymerase II core promoter. *Mol Cell Biol* 30: 3471-3479

Tsukiyama T, Wu C (1995) Purification and properties of an ATP-dependent nucleosome remodeling factor. *Cell* 83: 1011-1020

Tunnacliffe E, Corrigan AM, Chubb JR (2018) Promoter-mediated diversification of transcriptional bursting dynamics following gene duplication. *Proc Natl Acad Sci U S A* 115: 8364-8369

Venken KJ, He Y, Hoskins RA, Bellen HJ (2006) P[acman]: a BAC transgenic platform for targeted insertion of large DNA fragments in *D. melanogaster*. *Science* 314: 1747-1751

Vo Ngoc L, Kassavetis GA, Kadonaga JT (2019) The RNA Polymerase II Core Promoter in *Drosophila*. *Genetics* 212: 13-24

Wakimoto BT, Kaufman TC (1981) Analysis of larval segmentation in lethal genotypes associated with the antennapedia gene complex in *Drosophila melanogaster*. *Dev Biol* 81: 51-64

Wakimoto BT, Turner FR, Kaufman TC (1984) Defects in embryogenesis in mutants associated with the antennapedia gene complex of *Drosophila melanogaster*. *Dev Biol* 102: 147-172

Yokoshi M, Segawa K, Fukaya T (2020) Visualizing the Role of Boundary Elements in Enhancer-Promoter Communication. *Mol Cell* 78: 224-235 e225

Zabidi MA, Arnold CD, Schernhuber K, Pagani M, Rath M, Frank O, Stark A (2015) Enhancer-core-promoter specificity separates developmental and housekeeping gene regulation. *Nature* 518: 556-559

Zenklusen D, Larson DR, Singer RH (2008) Single-RNA counting reveals alternative modes of gene expression in yeast. *Nat Struct Mol Biol* 15: 1263-1271

Figure 1

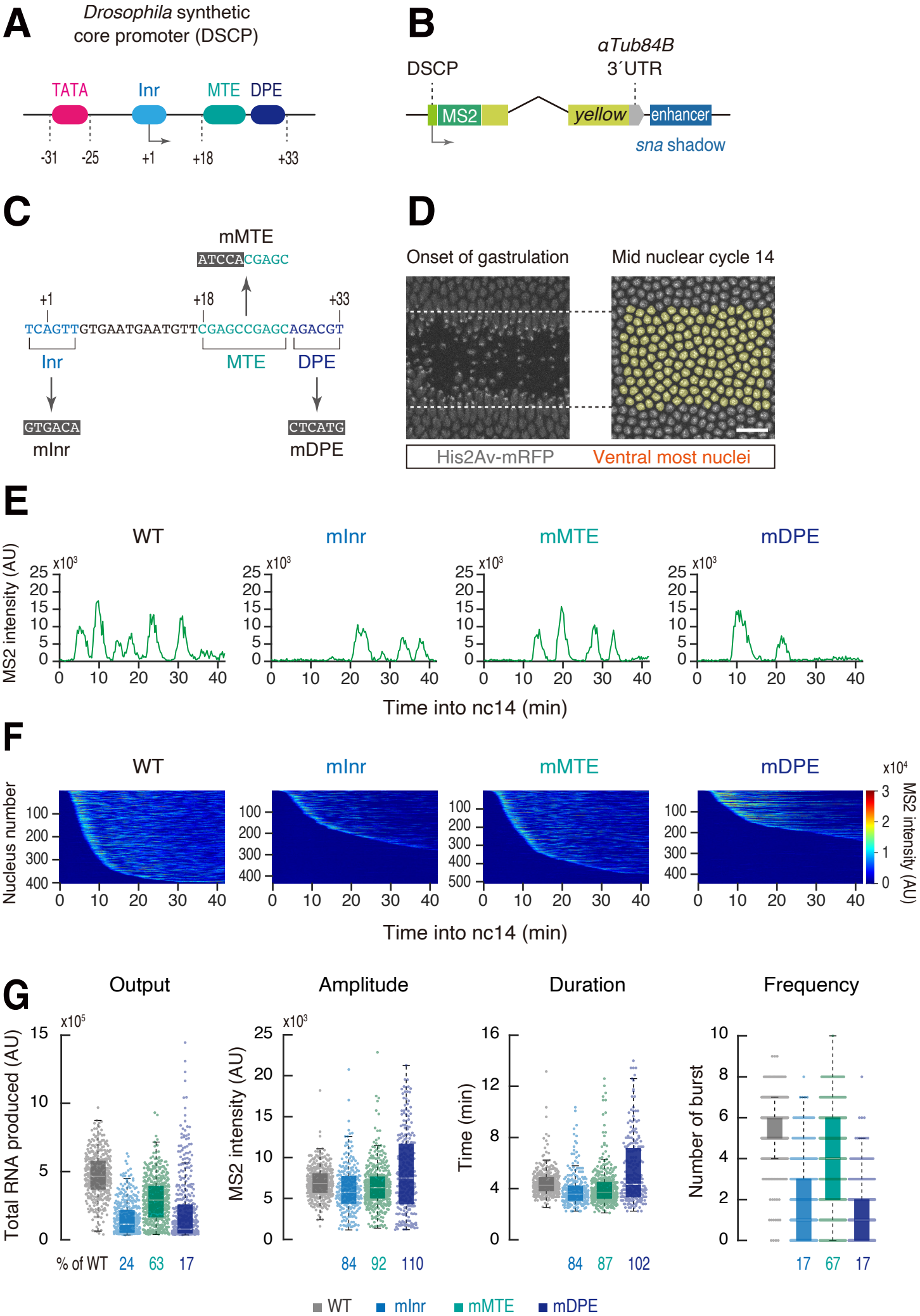
A
Drosophila synthetic core promoter (DSCP)
TATA
Inr
MTE
DPE
-31
-25
+1
+18
+33
B
DSCP
αTub84B 3´UTR
MS2
yellow
enhancer
sna shadow
C
mMTE
ATCCACGAGC
+1
+18
+33
TCAGTTGTGAATGAATGTTCGAGCCGAGCAGACGT
Inr
MTE
DPE
GTGACA
mInr
CTCATG
mDPE
D
Onset of gastrulation
Mid nuclear cycle 14
His2Av-mRFP
Ventral most nuclei
E
WT
mInr
mMTE
mDPE
MS2 intensity (AU)
x10³
Time into nc14 (min)
F
WT
mInr
mMTE
mDPE
Nucleus number
x10⁴
MS2 intensity (AU)
Time into nc14 (min)
G
Output
Amplitude
Duration
Frequency
Total RNA produced (AU)
x10⁵
MS2 intensity (AU)
x10³
Time (min)
Number of burst
% of WT
24
63
17
84
92
110
84
87
102
17
67
17
WT
mInr
mMTE
mDPE

Figure 2

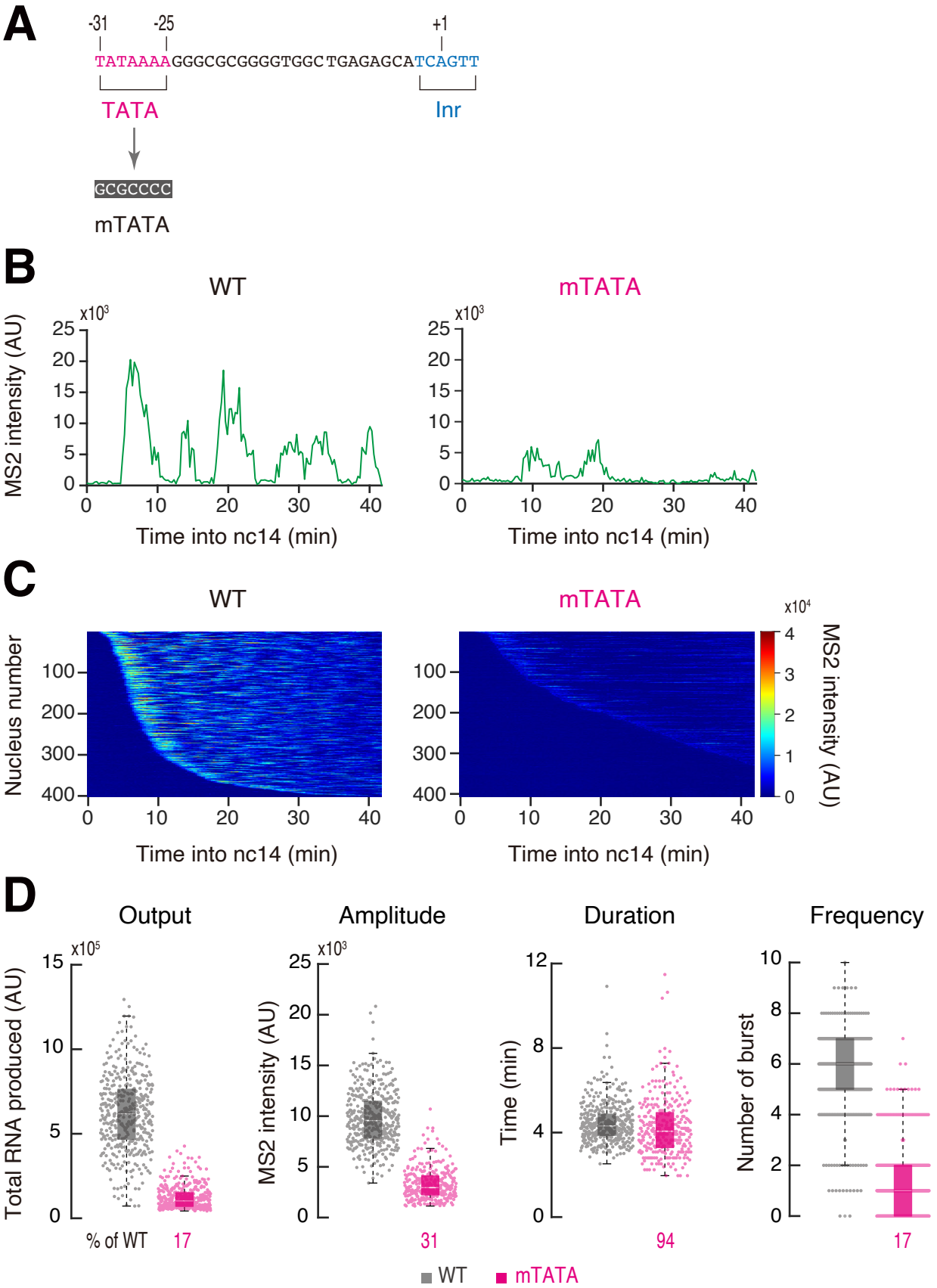
A
-31
-25
+1
TATAAAAGGGCGCGGGGTGGCTGAGAGCATCAGTT
TATA
Inr
GCGCCCC
mTATA
B
WT
mTATA
MS2 intensity (AU)
x10³
Time into nc14 (min)
C
WT
mTATA
Nucleus number
x10⁴
MS2 intensity (AU)
Time into nc14 (min)
D
Output
Amplitude
Duration
Frequency
Total RNA produced (AU)
x10⁵
MS2 intensity (AU)
x10³
Time (min)
Number of burst
% of WT
17
31
94
17
WT
mTATA

Figure 3

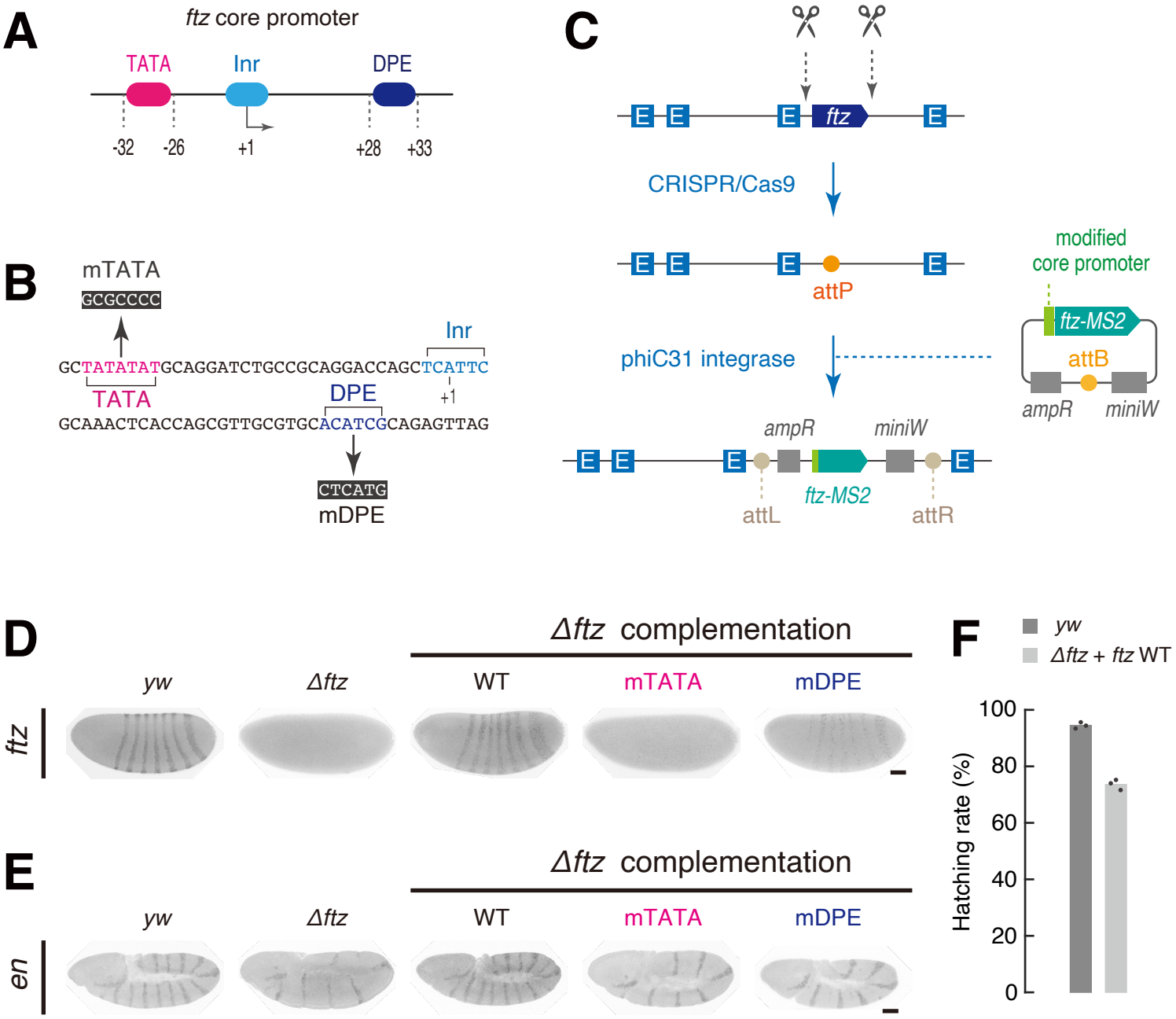
A
ftz core promoter
TATA
Inr
DPE
-32
-26
+1
+28
+33
B
mTATA
GCGCCCC
Inr
GCTATATATGCAGGATCTGCCGCAGGACCAGCTCATTC
TATA
DPE
+1
GCAAACTCACCAGCGTTGCGTGCACATCGCAGAGTTAG
CTCATG
mDPE
C
ftz
CRISPR/Cas9
attP
phiC31 integrase
modified
core promoter
ftz-MS2
attB
ampR
miniW
ampR
miniW
ftz-MS2
attL
attR
D
Δftz complementation
yw
Δftz
WT
mTATA
mDPE
ftz
E
Δftz complementation
yw
Δftz
WT
mTATA
mDPE
en
F
yw
Δftz + ftz WT
Hatching rate (%)
100
80
60
40
20
0

Figure 4

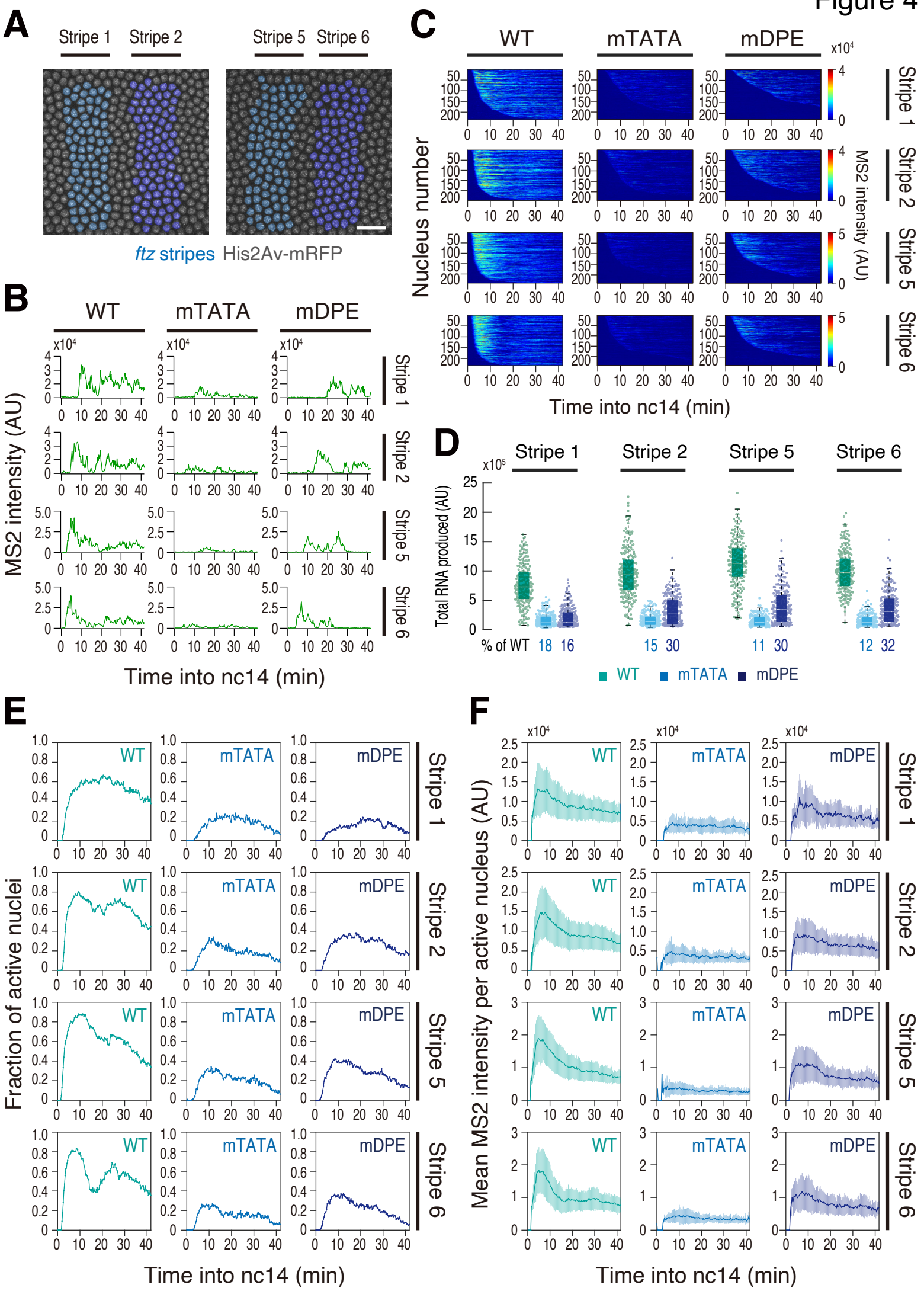
A
Stripe 1
Stripe 2
Stripe 5
Stripe 6
ftz stripes
His2Av-mRFP
B
WT
mTATA
mDPE
MS2 intensity (AU)
Stripe 1
Stripe 2
Stripe 5
Stripe 6
Time into nc14 (min)
C
WT
mTATA
mDPE
Nucleus number
MS2 intensity (AU)
Time into nc14 (min)
D
Stripe 1
Stripe 2
Stripe 5
Stripe 6
Total RNA produced (AU)
% of WT
18 16
15 30
11 30
12 32
WT
mTATA
mDPE
E
Fraction of active nuclei
Time into nc14 (min)
F
Mean MS2 intensity per active nucleus (AU)
Time into nc14 (min)

Figure 5

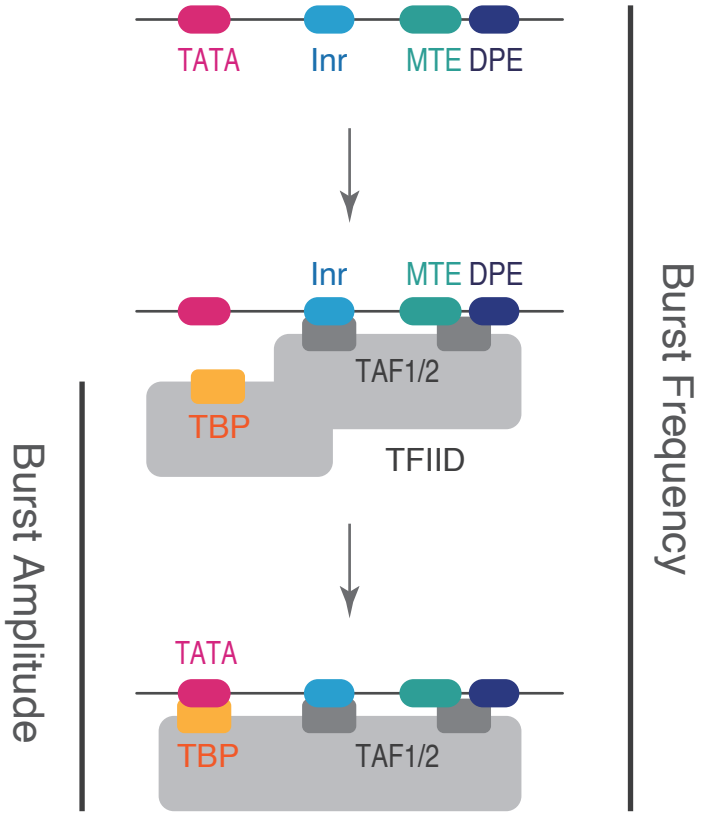
TATA
Inr
MTE
DPE
Inr
MTE
DPE
TAF1/2
TBP
TFIID
TATA
TBP
TAF1/2
Burst Frequency
Burst Amplitude

Figure EV1

A

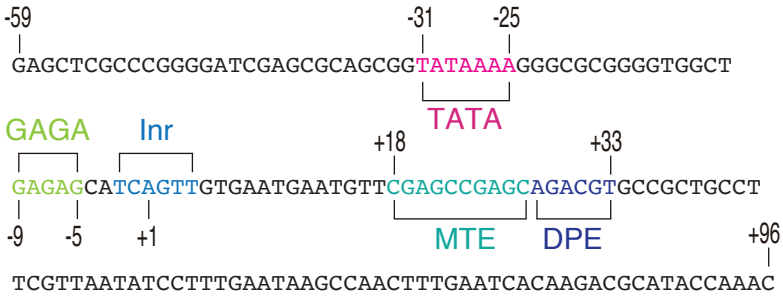

Drosophila synthetic core promoter (DSCP)

B

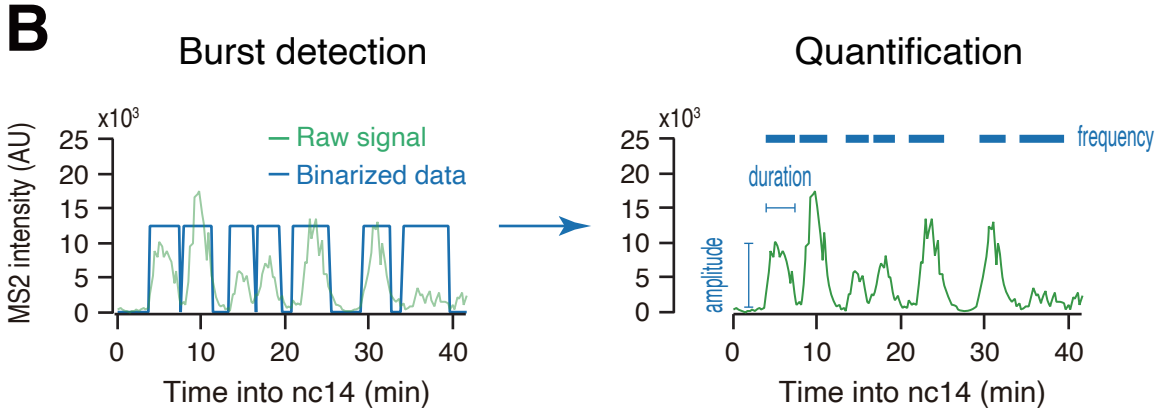

Figure EV1. Quantification of transcriptional bursting.

(A) Overall structure of the *Drosophila* synthetic core promoter (DSCP).

(B) Trajectory of transcription activity shown in Fig 1E (left). Amplitude and duration were measured for every single bursting event. Frequency was determined by counting total number of bursts during the analysis window.

Figure EV2

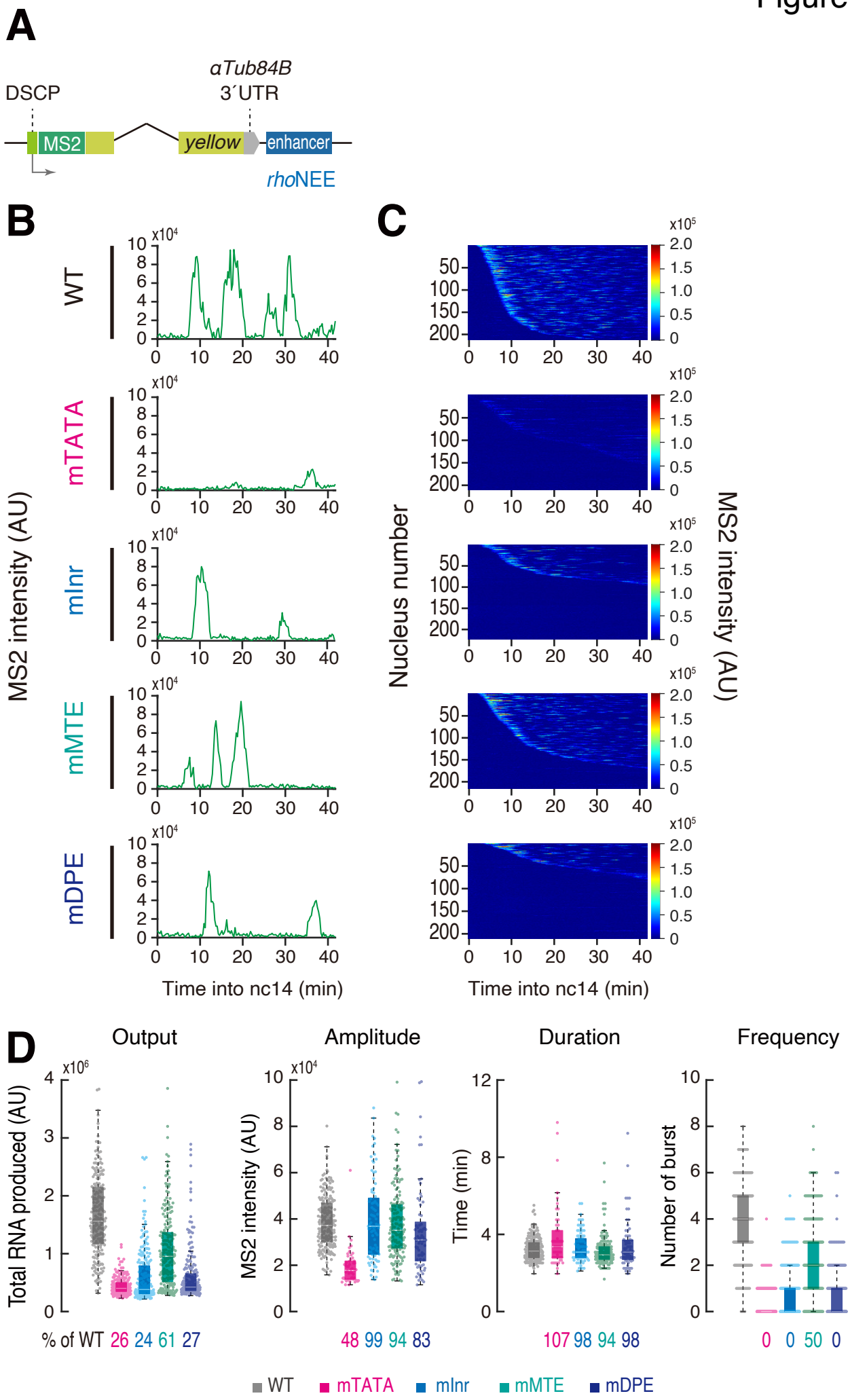
A
DSCP
αTub84B
3´UTR
MS2
yellow
enhancer
rhoNEE
B
WT
mTATA
mInr
mMTE
mDPE
MS2 intensity (AU)
Time into nc14 (min)
C
Nucleus number
MS2 intensity (AU)
Time into nc14 (min)
D
Output
Amplitude
Duration
Frequency
Total RNA produced (AU)
MS2 intensity (AU)
Time (min)
Number of burst
% of WT 26 24 61 27
48 99 94 83
107 98 94 98
0 0 50 0
WT
mTATA
mInr
mMTE
mDPE

Figure EV2. Live imaging analysis of reporter genes under the control of *rho*NEE.
(A) Schematic representation of the *yellow* reporter gene containing the 155-bp DSCP, the 666-bp *rho*NEE, and 24x MS2 RNA stem loops within the 5′ UTR.
(B) A representative trajectory of transcription activity of the MS2 reporter genes with WT DSCP (top), mTATA DSCP (upper middle), mInr DSCP (middle), mMTE DSCP (lower middle) and mDPE DSCP (bottom) in individual nuclei.
(C) MS2 trajectories for all analyzed nuclei. Each row represents the MS2 trajectory for a single nucleus. A total of 213, 211, 224, 216 and 210 nuclei located at the expression domain, respectively, were analyzed from three independent embryos for the reporter genes with WT DSCP (top), mTATA DSCP (upper middle), mInr DSCP (middle), mMTE DSCP (lower middle) and mDPE DSCP (bottom). All analyzed nuclei for each experiment were ordered by their onset of transcription in nc14.
(D) Boxplots showing the distribution of total output (left), burst amplitude (middle left), burst duration (middle right) and burst frequency (right). The box indicates the lower (25%) and upper (75%) quantile and the solid line indicates the median. Whiskers extend to the most extreme, non-outlier data points. A total of 213, 211, 224, 216 and 210 nuclei located at the expression domain, respectively, were analyzed from three independent embryos for the reporter genes with WT DSCP, mTATA DSCP, mInr DSCP, mMTE DSCP and mDPE DSCP. Relative median values normalized to the WT DSCP reporter are shown in bottom.

Figure EV3

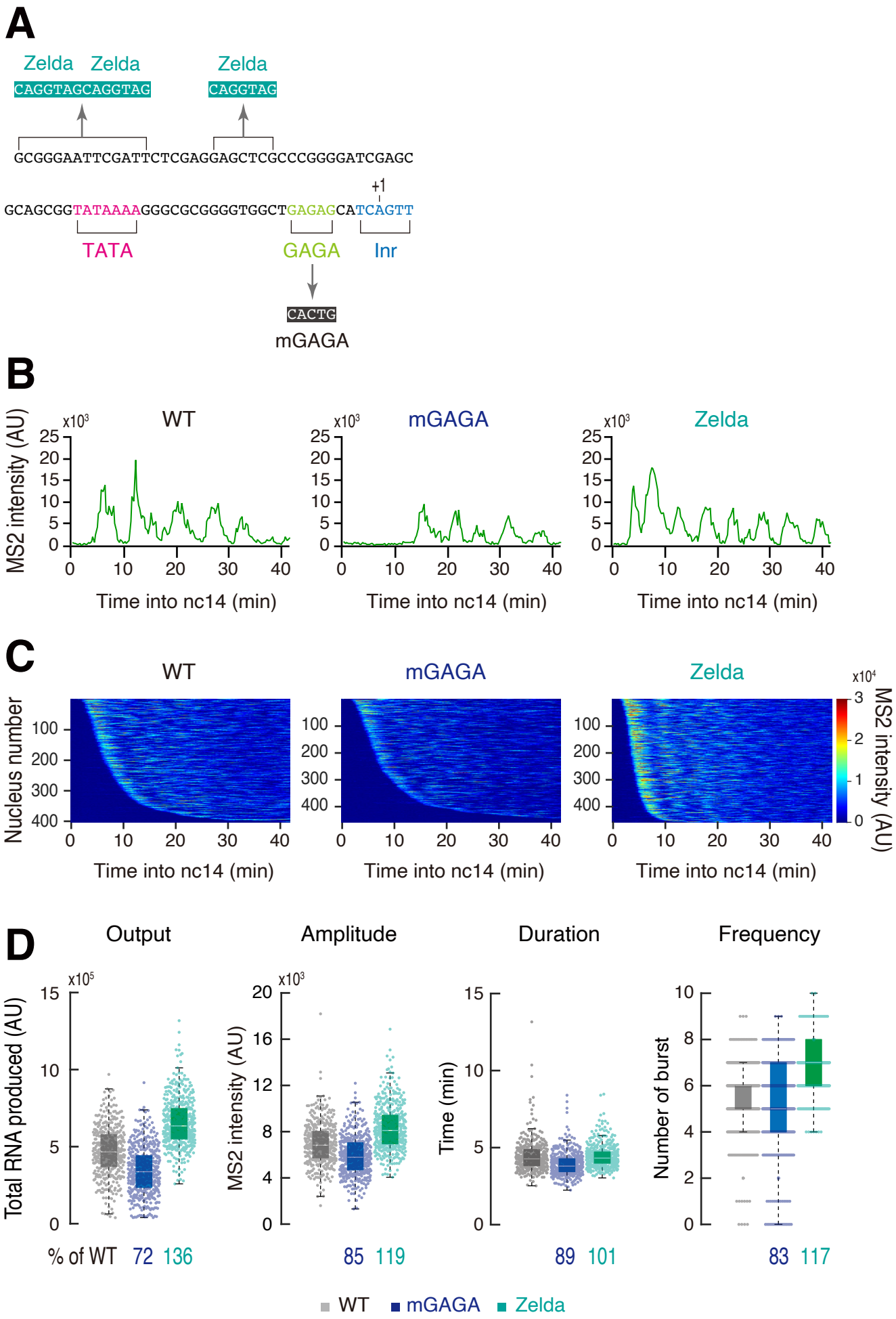
A
Zelda
Zelda
CAGGTAGCAGGTAG
Zelda
CAGGTAG
GCGGGAATTCGATTCTCGAGGAGCTCGCCCGGGGATCGAGC
+1
GCAGCGGTATAAAAGGGCGCGGGGTGGCTGAGAGCATCAGTT
TATA
GAGA
Inr
CACTG
mGAGA
B
WT
mGAGA
Zelda
MS2 intensity (AU)
x10³
Time into nc14 (min)
C
WT
mGAGA
Zelda
Nucleus number
Time into nc14 (min)
x10⁴
MS2 intensity (AU)
D
Output
Amplitude
Duration
Frequency
Total RNA produced (AU)
x10⁵
MS2 intensity (AU)
x10³
Time (min)
Number of burst
% of WT 72 136
85 119
89 101
83 117
WT
mGAGA
Zelda

Figure EV3. Promoter proximal GAGA and Zelda sites facilitate burst production.
(A) DSCP was modified to mutate GAGA site or add three optimal Zelda binding sites.
(B) A representative trajectory of transcription activity of the MS2 reporter genes with WT DSCP (left), mGAGA DSCP (middle) and Zelda DSCP (right) in individual nuclei.
(C) MS2 trajectories for all analyzed nuclei. Each row represents the MS2 trajectory for a single nucleus. A total of 403, 458 and 458 most ventral nuclei, respectively, were analyzed from three individual embryos for the reporter genes with WT DSCP (left), mGAGA DSCP (middle) and Zelda DSCP (right). All analyzed nuclei for each experiment were ordered by their onset of transcription in nc14. Panel of WT DSCP is the same as the panel in Fig 1F.
(D) Boxplots showing the distribution of total output (left), burst amplitude (middle left), burst duration (middle right) and burst frequency (right). The box indicates the lower (25%) and upper (75%) quantile and the solid line indicates the median. Whiskers extend to the most extreme, non-outlier data points. A total of 403, 458 and 458 most ventral nuclei, respectively, were analyzed from three individual embryos for the reporter genes with WT DSCP, mGAGA DSCP and Zelda DSCP. Relative median values normalized to the WT DSCP reporter are shown in bottom. Plot of WT DSCP is the same as the plot in Fig 1G.

Figure EV4

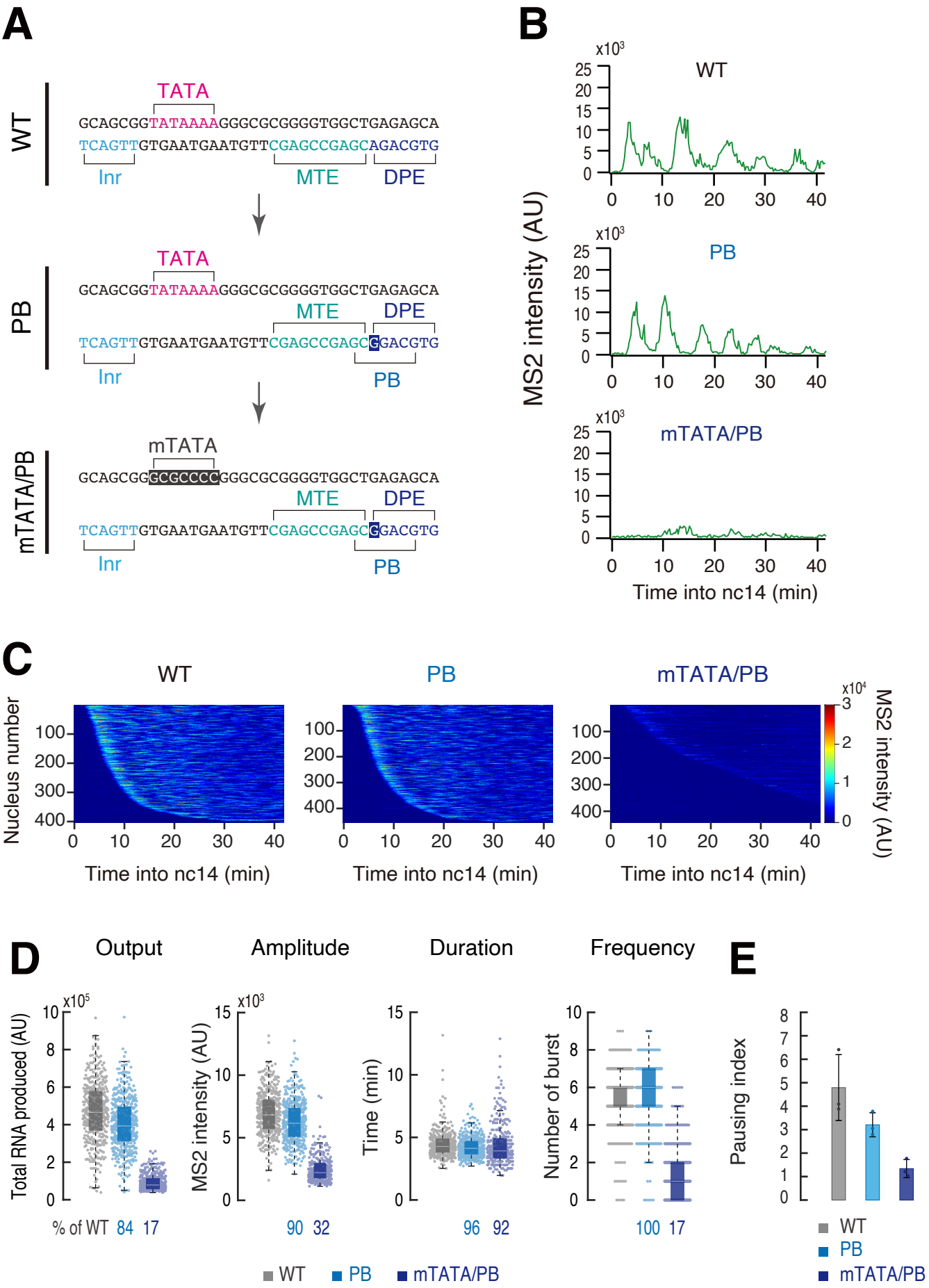
A
WT
TATA
GCAGCGGTATAAAAGGGCGCGGGGTGGCTGAGAGCA
TCAGTTGTGAATGAATGTTCGAGCCGAGCAGACGTG
Inr
MTE
DPE
PB
TATA
GCAGCGGTATAAAAGGGCGCGGGGTGGCTGAGAGCA
MTE
DPE
TCAGTTGTGAATGAATGTTCGAGCCGAGCGGACGTG
Inr
PB
mTATA/PB
mTATA
GCAGCGGGCGCCCCGGGCGCGGGGTGGCTGAGAGCA
MTE
DPE
TCAGTTGTGAATGAATGTTCGAGCCGAGCGGACGTG
Inr
PB
B
MS2 intensity (AU)
WT
PB
mTATA/PB
Time into nc14 (min)
C
WT
PB
mTATA/PB
Nucleus number
Time into nc14 (min)
MS2 intensity (AU)
D
Output
Amplitude
Duration
Frequency
Total RNA produced (AU)
MS2 intensity (AU)
Time (min)
Number of burst
% of WT 84 17
90 32
96 92
100 17
WT
PB
mTATA/PB
E
Pausing index
WT
PB
mTATA/PB

Figure EV4. TATA mutation diminishes burst amplitude independently of Pol II pausing.

(A) DSCP was modified to contain PB motif at +26 to +32 positions relative to the TSS.

(B) A representative trajectory of transcription activity of the MS2 reporter genes with WT DSCP (top), PB DSCP (middle) and mTATA/PB DSCP (bottom) in individual nuclei.

(C) MS2 trajectories for all analyzed nuclei. Each row represents the MS2 trajectory for a single nucleus. A total of 403, 454 and 442 ventral most nuclei, respectively, were analyzed from three independent embryos for the reporter genes with WT DSCP (left), PB DSCP (middle) and mTATA/PB DSCP (right). All analyzed nuclei for each experiment were ordered by their onset of transcription in nc14. Panel of WT DSCP is the same as the panel in Fig 1F.

(D) Boxplots showing the distribution of total output (left), burst amplitude (middle left), burst duration (middle right) and burst frequency (right). The box indicates the lower (25%) and upper (75%) quantile and the solid line indicates the median. Whiskers extend to the most extreme, non-outlier data points. A total of 403, 454 and 442 ventral most nuclei, respectively, were analyzed from three independent embryos for the reporter genes with WT DSCP, PB DSCP and mTATA/PB DSCP. Relative median values normalized to the WT DSCP reporter are shown in bottom. Plot of WT DSCP is the same as the plot in Fig 1G.

(E) qPCR quantification of ChIP experiments using Pol II antibody. The Pol II occupancy was quantified at the promoter region and the gene body as percent ChIP signal normalized to corresponding sample-specific ChIP inputs. Pausing Index was determined as a ratio of Pol II occupancy at the core promoter region to the gene body. Each dot represents measurement from a single experiment. Error bars represent the standard deviation of the mean of three independent experiments.

Figure EV5

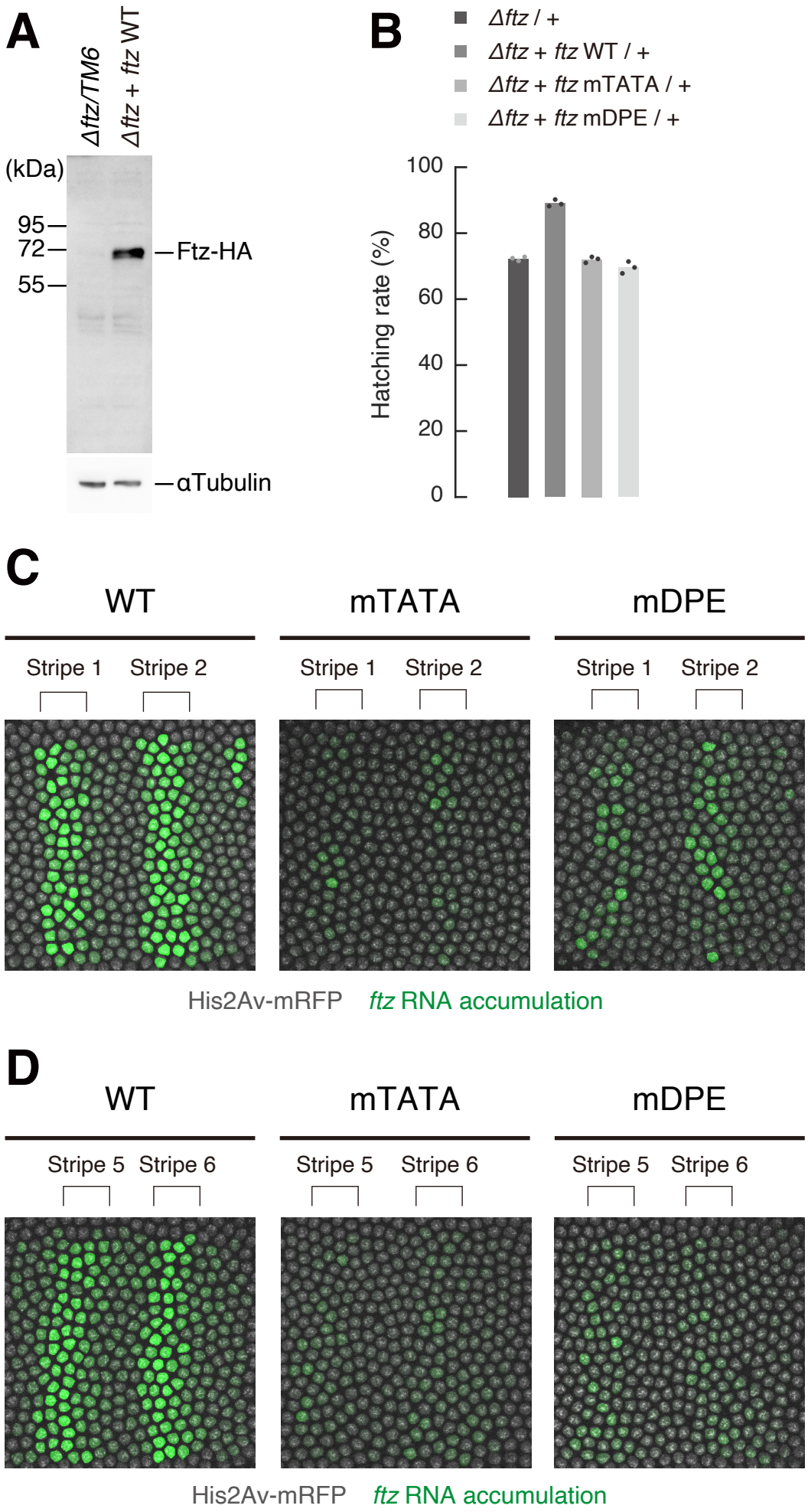
A
Δftz/TM6
Δftz + ftz WT
(kDa)
95
72
55
Ftz-HA
αTubulin
B
Δftz / +
Δftz + ftz WT / +
Δftz + ftz mTATA / +
Δftz + ftz mDPE / +
Hatching rate (%)
100
80
60
40
20
0
C
WT
mTATA
mDPE
Stripe 1
Stripe 2
His2Av-mRFP
ftz RNA accumulation
D
WT
mTATA
mDPE
Stripe 5
Stripe 6
His2Av-mRFP
ftz RNA accumulation

Figure EV5. TATA and DPE mutations lead to sporadic stripe formation.

(A) Expression of Ftz protein was confirmed by western blotting. 2-4 h embryos laid by each genotype were collected and used for the analysis.

(B) Hatching rates of eggs laid by *Δftz-attP/+*, *ftz WT core promoter-ftz-HA-24xMS2/+*, *ftz mTATA core promoter-ftz-HA-24xMS2/+*, and *ftz mDPE core promoter-ftz-HA-24xMS2/+* lines. In this experiment, one fourth of resulting embryos are expected to be homozygous mutants. Each dot represents measurement from a single experiment. For each trial, 500 embryos were analyzed per genotype.

(C) Computational reconstitution of *ftz* mRNA accumulation at the anterior stripe region. Scale bar indicates 20 μm.

(D) Computational reconstitution of *ftz* mRNA accumulation at the posterior stripe region. Scale bar indicates 20 μm.

Movie Legends

Movie EV1. Live imaging of the MS2 reporters with WT, mInr, mMTE and mDPE DSCP.

Live imaging of *MS2-yellow-sna shadow enhancer* containing WT (left), mInr (left middle), mMTE (right middle) and mDPE DSCP (right) during nc14. Each nucleus was false-colored with the intensity proportional to the instantaneous MS2 signal at a given time in a given nucleus. The maximum projected image of His2Av-mRFP is shown in gray. Images are oriented with ventral view facing up.

Movie EV2. Live imaging of the MS2 reporters with WT and mTATA DSCP.

Live imaging of *MS2-yellow-sna shadow enhancer* containing WT (left) and mTATA DSCP (right) during nc14. Each nucleus was false-colored with the intensity proportional to the instantaneous MS2 signal at a given time in a given nucleus. The maximum projected image of His2Av-mRFP is shown in gray. Images are oriented with ventral view facing up

Movie EV3. Live imaging of *ftz-MS2* complementation alleles.

Live imaging of *ftz-MS2* containing WT (top), mTATA (middle) and mDPE core promoter (bottom) during nc14. Anterior stripe 1 and 2 regions were shown in left. Posterior stripe 5 and 6 regions were shown in right. Each nucleus was false-colored with the intensity proportional to the instantaneous MS2 signal at a given time in a given nucleus. The maximum projected image of His2Av-mRFP is shown in gray. Images are oriented with anterior to the left.